Testing of centrifugal filter devices as a tool to quantify protein-nanoparticle interactions using UV/Vis measurements

by

Ana Carolina Bohórquez

A thesis submitted in partial fulfillment of the requirements for the degree of

MASTER OF SCIENCE
in
CHEMICAL ENGINEERING

UNIVERSITY OF PUERTO RICO
MAYAGÜEZ CAMPUS
2012

Approved by:

_____	_____
Magda Latorre Esteves, Ph.D. President, Graduate Committee	Date
_____	_____
Carlos Rinaldi, Ph.D. Member, Graduate Committee	Date
_____	_____
Madeline Torres-Lugo, Ph.D. Member, Graduate Committee	Date
_____	_____
Francisco M. Monroig Saltar, Ph.D Graduate School Representative	Date
_____	_____
Aldo Acevedo-Rullán, Ph.D. Chairperson of the Department	Date

ABSTRACT

Centrifugal Filter Devices (CFD) has been tested for the quantification of protein adsorption onto the surface of magnetic nanoparticles coated with biocompatible polymers. Using a phosphate buffered saline wash protocol, the bicinchoninic acid assay (BCA), and mass balance calculations, the amount of protein adsorbed was calculated. The iron in magnetic cores interferes with the BCA assay because it remains in the supernatant after centrifugation. CFD was considered an attractive alternative, because in principle it could retain colloidally stable nanoparticles, leaving unbound protein to be quantified in the filtrate. Magnetic nanoparticles were synthesized by co-precipitation and grafted with Carboxylmethly Dextran or silanized polyethylene glycol. Proteins used for this study include anionic and cationic proteins: Bovine Serum Albumin and Lysozyme from Hen Egg White, respectively. In conclusion, CFDs were not suitable for the study of protein-nanoparticle interactions because membrane fouling and concentration polarization were encountered; critical factors that compromised measurement accuracy.

RESUMEN

Dispositivos de Filtro para Centrifugación (CFD) fueron evaluados para la cuantificar la adsorción de proteínas sobre la superficie de nanopartículas magnéticas recubiertas con biopolímeros. Utilizando un protocolo de enjuague, el método del ácido bicinconínico (BCA), y cálculos de balance de masa fue estimada la proteína adsorbida. El hierro de los núcleos magnéticos interfiere con el ensayo BCA porque trazas permanecen en sobrenadantes después de centrifugar, por ello CFDs se consideraron atractivos al retener nanopartículas coloidalmente estables; dejando proteínas libres en el filtrado para ser cuantificadas. Nanopartículas fueron sintetizadas vía co-precipitación y cubiertas con carboximetil dextrano o polietilenglicol silanizado. Las proteínas utilizadas incluyen proteínas aniónicas y catiónicas, Albúmina de Suero Bovino (BSA) y la Lisozima de Huevo de Gallina (LYZ), respectivamente. En conclusión, los CFDs no son recomendables para estudiar interacciones proteína-nanopartícula porque factores como el ensuciamiento de la membrana y polarización de la concentración afectan la precisión de las mediciones.

To my family in Venezuela

ACKNOWLEDGEMENTS

During my M.S. studies several people collaborated with me on my research. I want to thank everyone that helped me to achieve this goal especially the following people,

Thanks to my advisor Dr. Magda Latorre-Esteves for your support and advice.

I want to express my sincere thanks to Dr. Carlos Rinaldi because he gave me the opportunity to do research under his guidance and supervision. Thank you so much for being patient with me during the last two years. Thanks for your support and exceptional dedication.

I am very happy to have met Prof. Antonio Esteves; a lot of thanks for your support. Thanks for telling me at the conference in El Salvador about the opportunities to study in Mayaguez. A few minutes talking with you were decisive in changing and opening my mind to have new directions and horizons in my professional life.

Thanks to my dear lab mate Roberto Olayo for his continuous support and helping me to characterize samples using ^{1}H-NMR, TEM, and GPC measurements. Roberto thanks a lot for your time explaining the principles of all these characterization techniques. Additionally, thanks for all your recommendations in using IGOR in order to analyze my data.

Mar Creixell and Vanessa Ayala, thanks for explaining and training me to prepare particles and modified polymers. Dear friends, the confidence and friendship that you gave me has played an important role for me this whole time.

Thanks to Dr. Adriana Herrera, and the Postdocs Fellows Dr. Jeremiah Hubbard and Dr. Lenibel Santiago-Rodriguez, because they helped me to figure out synthesis, and characterization procedures. Additionally, thanks Jere and Leni for your honest and invaluable friendship and support during my Puerto Rican life.

A special thanks to the people that form part of my life, and have a piece of my heart: my dear cousin Lisbeth Pais, my childhood friend Jennifer Pereira, my high school friends Daiany Palacios, Gleidy Mendoza, Carlos Luis Quijada, and Jhon Pulido; my undergraduate school friends Yulyanna Carrasco and Mayra Mujica. Thanks for keeping in touch despite of the distance.

Finally, I wish to acknowledge the Chemical Engineering Department for giving me the opportunity to study at the University of Puerto Rico at Mayagüez and the NSF Center for Research Excellence in Science and Technology (CREST) for the financial support.

TABLE OF CONTENTS

LIST OF TABLES

Page

LIST OF FIGURES

Page

1 INTRODUCCION

1.1 Motivation

Magnetic nanoparticles are currently being studied and employed in biomedical applications such as diagnosis via Magnetic Resonance Imaging (MRI) [1], protein separation, and for the treatment of diseases such as cardiovascular disease, neurological disorders, and cancer [2], [3]. Biomedical applications of nanotechnology are concentrated in *in vitro* studies. However, the importance of nanotechnology in medicine has increased notably in the last few years because of its potential for drug delivery due to the selective uptake of coated nanoparticles in certain tissues [4]. However, these applications are all limited by non-specific protein adsorption, where proteins non-covalently bind to nanoparticles [5]. To gain a better understanding of this phenomenon, *in vivo* studies are necessary in order to study the pharmacokinetics, biodistribution, and behavior of proteins adsorbed onto nanoparticle surfaces [6].

There is a lack of understanding of how nanoparticle surface chemistry can influence interactions with common proteins that are present in the bloodstream, such as the plasma proteins albumin, transferrin, α, β, and γ immunoglobulins, myoglobin and fibrinogen [7], and [8]. Plasma proteins play an important role in transportation of nutrients for *in vivo* systems. Protein adsorption of plasma proteins onto nanoparticle surfaces is important in determining the biocompatibility of nanomaterials and in manipulating protein adsorption in biomedical applications. This requires a detailed understanding of the mechanism of protein adsorption onto nanoparticle surfaces.

Bovine Serum Albumin (BSA) was one of the model proteins selected to study its interaction with magnetic nanoparticles. BSA possesses negative surface charge at physiological pH (~7.4) due to the presence of aspartic and glutamic amino acids. Hen Egg White Lysozyme (LYZ) was incorporated into the study as a model protein with positive surface charge. The positive potential of LYZ is due to the basic amino acids lysine, arginine and histidine [9] and [10].

The amount of protein adsorbed onto nanoparticle surface was calculated using a phosphate buffered saline wash protocol with Centrifugal Filter Devices (CFDs), the bicinchoninic acid spectrophotometry assay (BCA), and mass balance calculations. Results helped clarify the effect of surface charge on the adsorption of proteins onto the surface of PEGSilane coated nanoparticles (almost neutral surface charge at physiological conditions) and Carboxymethyl Dextran (CMDx) coated nanoparticles (negative surface charge at physiological conditions).

2 BACKGROUND

2.1 Iron oxide magnetic nanoparticles

Iron oxide nanoparticles with a wide particle size distribution are usually synthesized by the co-precipitation of iron salts using ammonium hydroxide in an aqueous media to obtain a mix between magnetite (Fe_3O_4) and maghemite (γFe_3O_4) iron oxides, which are too difficult to distinguish because their diffraction spectra is too similar [11], [12]. This method was first proposed by Massart [13] who studied parameters such as strength of base, pH conditions, and Fe^{+3}/Fe^{+2} ratio on the effect of the yield of the coprecipitation reaction and particles sizes. Massart concluded that the size decreases as the pH, Fe^{+3}/Fe^{+2} ratios, and ionic strength in the medium increases. Figure 1 shows a common co-precipitation setup that included a temperature controller, reactor, rotor, N_2 flux and a pH meter.

Figure 1. Co-precipitation synthesis setup under N_2 controlled atmosphere.

There are other methods reported to synthesize magnetic nanoparticles, such as Hot-Injection and Heat-Up methods. Monodisperse particles with significant size control, and high crystallinity, can be achieved using high temperature methods. Typically, for these methods iron complexes are decomposed in the presence of surfactants and organic solvents. The high temperatures used and the nature of the solvent result in magnetic nanoparticles with suitable size, size distribution and high cristallinity [12], [14], and [15].

Reports in the literature suggest that the process of magnetic nanoparticle synthesis consists of two steps. The first is a short single burst nucleation, followed by growth of the nuclei [15]. The overall size and size distribution of magnetic nanoparticles are an important consideration, as this can affect biocompatibility and biodistribution *in vivo* [12]. In order to maximize the amount of nanoparticles synthesized in the experiments, the co-precipitation method will be used because of the low cost and large amount of nanoparticles obtained.

2.2 PEGSilane polymers

PEGSilane is a functional polymer. It has the advantage of combining oxidized Polyethylene glycol (PEG) and 3-aminopropyl triethoxysilane (APS) through a high temperature amidation reaction in order to covalently bond the amino groups present in the silane molecule to carboxylic groups in the oxidized PEG (mPEG-COOH). The preparation of PEG-Silane polymers is a straightforward procedure, but has the disadvantage that APS molecules in a stochiometric proportion do not react totally with the oxidized PEG.

The use of silanated polymers for surface modification might have advantages over using other conventional methods. Silanated polymers can simplify modification procedures with fewer steps [16]. Barrera et al [17] demonstrated that the steric repulsion between PEGSilane chains in the coated particles was responsible for nanoparticle stabilization, making these nanoparticles appropriate for biomedical applications.

Larsen et al. [18] have performed a ligand exchange reaction in toluene solvent in the presence of the base triethylamine and water with commercially available PEGSilane with a molecular weight distribution of 596-725 Da. This report explained the mechanism of reaction, where water converts the $Si(OMe)_3$ to the silanol form, enabling efficient reaction with the oxygen on the iron oxide particles surface and oleic acid replacement. The silanol forms polymer networks of up to three binding sites per Si atom to the iron oxide, resulting in a more stable coat compared to oleic acid because oleic acid is only adsorbed onto the surface. The PEGSilane coated particles obtained had low toxicity and stability, and were used for *in vivo* applications in order to study size-dependent accumulation in Murine tumors.

2.3 Carboxymethyl Dextran with different degrees of substitution of carboxylic groups polymers

Dextran is a linear polysaccharide consisting of repeating units of D-glucose linked together by glycosidic bonds. The hydroxylic groups of the dextran sugar backbone confer the polymer with a hydrophilic nature and versatility for coupling to other molecules, such as markers and proteins using standard amine-carboxylate coupling methods [19]. Dextran has been used to modify magnetic nanoparticles for biomedical applications due to its low toxicity and suitability for suspensions in cell culture media and biological buffers [11].

The groups on each glucose monomer can be oxidized to carboxylic groups in the presence of monocloroacetic acid. The classical conditions employ the reaction of monocloroacetic (MCA) with Dextran in water under strong alkaline conditions. MCA in the presence of NaOH reacts with dextran to produce Carboxymethyldextrane (CMDx) according to the following reaction scheme [20]:

$$\mathrm{Dx-OH + ClCH_2 + 2NaOH \rightarrow Dx-OCH_2COONa + NaCl}$$

At the same time, MCA reacts with NaOH to give glycolic acid as a by-product.

$$\mathrm{ClCH_2COOH + NaOH \rightarrow OH-CH_2COOH + NaCl}$$

From this information, it can be deduced that the carboxymethylation reaction depends on NaOH concentration, reaction medium, [MCA]/ [dextran] ratio, temperature, molecular weight, and duration of the reaction. It was confirmed that these factors control the yield of carboxylic groups in the dextran chain.

2.4 Surface modification of magnetic nanoparticles

The surface modification of magnetic nanoparticles depends on the synthesis method. An efficient and stable approach to attach polymers onto the surface of magnetic nanoparticles involves two initial procedures: (i) condensation, or (ii) ligand exchange of silane compounds with specific functionalities. On a regular basis, condensation processes are performed when magnetic nanoparticles are synthesized by the co-precipitation method [11]. The ability of silanes to bind to –OH groups is a spontaneous and slow procedure.

On the other hand, when surfactants such as oleic acid (OA), rinoleic acid, etc., are incorporated into a synthesis in order to enhance monodispersity and size distribution of nanoparticles, a ligand exchange is a common procedure to attach the silane compounds onto the magnetic cores [21].

Silanes are bifunctional compounds that can be used to attach one substance to another. They have been used for many years as adhesive agents to promote bonding of an inorganic layer to an organic layer. Iron is a common inorganic substrate used with silane coupling agents for efficient and stable modifications [19]. For this reason, silane compounds have been increasingly reported as being important functionalization agents for magnetic nanoparticles in order to incorporate polymer chains onto metal surfaces. Different silanes have a wide variety of end groups such as PEG, aldehyde, cyano, amine or carboxylic acid groups to make water dispersible nanoparticles.

Nanoparticle surface modification using polymeric materials improves biocompatibility, transport, and retention. Polyethylene glycol (PEG) improves nanoparticle stability in biological systems. PEG has a wide array of properties that makes it suitable for biomedical applications, such as biocompatibility, biodegradability, low toxicity, solubility in aqueous solution, and low immunogenicity. In this work, PEGSilane will be covalently attached to oleic acid-coated magnetic nanoparticles. The covalent attachment of PEG can "mask" the therapeutic agent from the host's immune system and increase its hydrodynamic size, which prolongs bloodstream circulation time and reduces non-specific interactions with plasma proteins for *in vivo* applications.

Herrera et al. [22] functionalized magnetite nanoparticles with carboxymethyldextran covalently attached onto the particles surface to prevent losses of dextran chains in suspension with biological buffers. In this instance, carboxylic groups present in the carboxymethyldextran molecule were activated via EDC (1-Ethyl-3-(3-dimethylaminopropyl) - Diisopropylcarbodiimide)/ NHS (N-Hydroxysuccinimide) chemistry in order to react with amine end groups previously grafted onto the magnetic cores by condensation of aminopropylsilane molecules. Highly stable suspensions of magnetite nanoparticles with electrostatic and steric repulsion and no observable particle precipitation at the studied pH range were produced. In addition, CMDx coated nanoparticles will be synthesized in this project in order to compare protein adsorption using PEGSilane coated nanoparticles.

2.5 Colloidal stability of magnetic nanoparticles for potential uses in biomedical applications

Magnetic nanoparticles in suspension may adhere together and form aggregates of increasing size which may settle out due to gravity or strong electrostatic interactions between proteins and electrolytes in cell culture media, biological buffers, and water. At specific pH conditions electrolytes and proteins could be absorbed onto the particle surface and neutralize the polymer layers that stabilize the particles [23]. Also, this stability could be disrupted upon exposure to

changes such as temperature (for example sterilization at 121 ºC), ionic strength, or in the presence of an external magnetic field (for magnetic measurements or emergent therapies such as Magnetic Fluid Hyperthermia). The majority of biomedical applications require a stable suspension of magnetic nanoparticles in a liquid carrier such as: phosphate buffered saline (PBS), N-(2-Hydroxyethyl) piperazine-N′-(2-ethanesulfonic acid) (HEPES) buffer, sodium chloride at 0.9%, eagle's minimum essential medium (EMEM), dulbecco's modified eagle's medium (DMEM) and RPMI 1640 medium.

In the 1940s, Derjaguin, Verway, Landau and Overbeek developed a theory that dealt with colloidal stability (DLVO). This theory suggests that the stability of a colloidal system is determined by the sum of the potential energy due to the solvent, van der Waals attractive forces, and electrical double layer repulsive forces that exist between particles as they approach each other due to the Brownian motion they are undergoing [24]. The DLVO theory proposes that an energy barrier resulting from the repulsive force prevents two particles approaching one another and adhering together. However, if the particles collide with sufficient energy to overcome that barrier, the attractive force will pull them into contact, where they adhere strongly and irreversibly together. Therefore if the particles have sufficiently high repulsion, the dispersion will resist flocculation and the colloidal system will be stable. Figure 2 shows a representation of the DLVO theory explanation:

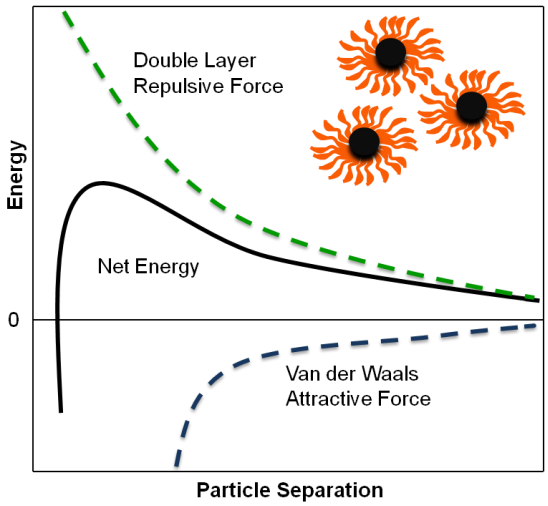

Figure 2. Variation of free energy with particle separation according to DLVO theory.

Therefore, to maintain the stability of a colloidal system, the repulsive forces must be dominant, and colloidal stability is achieved through two fundamental mechanisms. The first is steric repulsion, which involves polymers added to the system adsorbing or covalently bonding onto the particle surface and preventing the particle surfaces from coming into close contact. If enough polymer adsorbs or covalently attaches onto the nanoparticle, the thickness of the coating is sufficient to keep particles separated by steric repulsions between the polymer layers, and at those separations the Van der Waals forces are too weak to cause the particles to adhere. The second is electrostatic or charge stabilization, which affects particle interactions due to the distribution of charged species in the system, as is the case of CMDx coated nanoparticles with different degrees of COO- substitution [25].

Creixell et al [11] performed a study demonstrating how the grafting method of CMDx onto the magnetic nanoparticles affects the colloidal stability in biological buffers and cell culture media. This study suggests colloidal stability is affected by the presence of salts in biological buffers, which have different effects in adsorbed versus covalently bound polymer chains. Salts displaced adsorbed, but not covalently bonded polymer chains. This resulted in partial aggregation and agglomeration of nanoparticles coated with adsorbed polymer, which was observable against time or increases in temperature.

The influence of the composition of the polymer coating and nanoparticle surface charge on the colloidal stability of these particles in different cell media was studied by Petri-Fink et al [26]. In this work, authors tried to establish correlations between cytotoxicity or uptake rates and agglomeration behavior of polyvinyl alcohol (PVA)-, vinyl alcohol/vinyl amine copolymer (A-PVA), and polyethylenimine (PEI) coated superparamagnetic iron oxide nanoparticles. This correlation played a key role in the design of simplified toxicity tests and for the further development of such particles for *in vivo* applications. For *in vitro* studies Petri-Fink and collaborators confirmed each nanoparticle system has to be considered individually since cell uptake, and to certain extent cytotoxicity, was not only dependent on particle size and surface

chemistry, but also highly dependent on cell lines. There is also a significant influence of the medium and the presence and absence of serum on particle internalization in cells.

2.6 Blood stream proteins

Blood is an essential fluid that carries out the critical functions of transporting oxygen and nutrients to the cells and getting rid of carbon dioxide, ammonia, and other waste products. Also, it plays a pivotal role in the immune system and in maintaining a constant body temperature. There are thousands of blood components but four of the most important ones are erythrocytes (red cells), leucocytes (white cells), thrombocytes (platelets), and plasma. These components are distributed in 55% plasma, and 45% formed elements (99% red cells and 1% white cells + platelets).

There are a variety of pathways by which a foreign particle enters the human bloodstream. When nanoparticle interaction with blood system occurs, plasma proteins will immediately adsorb to the material surface, forming a protein-corona that changes vs. time [27]. Depending on nanoparticle surface properties, certain proteins will predominately attach to it and this behavior plays a pivotal role in biodistribution *in vivo*. The competitive adsorption of proteins onto nanoparticles in plasma was first described by Vroman (1962), therefore being known as the "Vroman effect" [28], and [29].

Human blood plasma contains many proteins that perform various housekeeping functions, such as participating in molecular transport, signaling cascades and regulatory events [30]. A list of the most common proteins found in human blood plasma is described below:

Human Serum Albumin (HSA) is a large globular protein. In human plasma, albumin has a concentration in the order of 0.63 mM with a molecular weight of 66.5 kDa, and is similar to other plasma proteins synthesized in the liver. Albumin in the liver is produced at a rate of

approximately 0.7 mg/h for every gram of liver. Currently, the accumulation of albumin in solid tumors is a novel mechanism for developing albumin-based drug delivery systems for tumor targeting [31], and [32].

Transferrin (TRANS) is an iron transport glycoprotein that controls the level of free iron in biological fluids, binding circulating iron and transporting it to a range of cell types. In addition, transferrin plays a defensive role against systemic infections by inhibiting iron from interacting with potential pathogens. Significant progress has been made towards expanding human transferrin applications in biotechnology and medicine, notably its use as a novel carrier system for targeted drug delivery [33].

Immunoglobulins are mainly used by the immune system as cell-surface receptors for antigens and soluble effector molecules, which permit cell signaling and cell activation, and can individually bind and neutralize antigens at a distance, respectively. IgG is the predominant immunoglobulin found in the body and it has an important role in the clearance of opsonized pathogens [34].

Fibrinogen (FIBR) plays a central role in the mechanism of blood coagulation and inflammatory pathways as a response of the innate immune system [35].

Lysozyme (LYZ) is a small protein with a low activity levels in the blood serum at concentrations between 7-13mg/mL, and forms part of the innate immune system. It is more abundant in a number of secretions, such as tears, saliva, and mucus [36], and [37]. Kokoshis et al. (1978) concluded LYZ is able to enhance the phagocytic activity of both polymorphonuclear leukocytes and macrophages [38].

Figure 3 shows an illustration by David Goodsell of a cross-section through the blood, with blood serum in the right half and a red blood cell in the left half. In the serum, are presented Y-

shaped antibodies, long thin fibrinogen molecules (in light red) and many small albumin proteins (yellow). The large UFO-shaped (Unidentified Flying Object shaped) objects are low density lipoprotein and the six-armed protein is complement C1. The red blood cell is filled with hemoglobin, in red. The cell wall, in purple, is braced on the inner surface by long spectrin chains connected at one end to a small segment of actin filament. Blood plasma contains ~80 mg/mL of protein, a concentration sufficient to cause significant crowding effects.

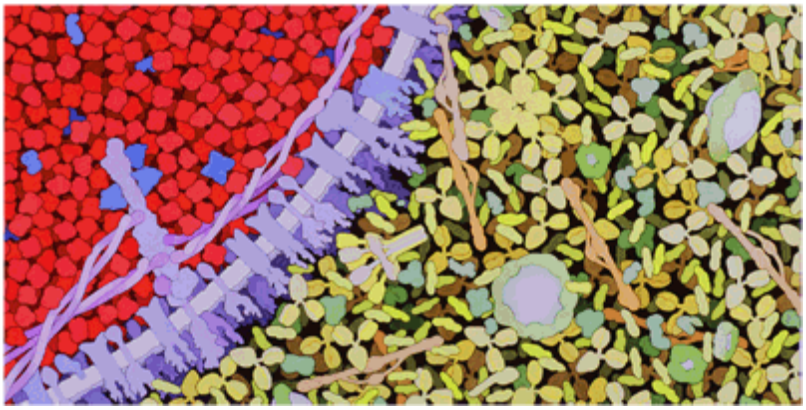

Figure 3. Blood serum and a red blood cell © David S. Goodsell 2000.

Table 1 shows a summary of the properties and physiological functions of the most common blood plasma proteins.

Table 1. Basic components of human blood

Protein	Molecular weight	Concentration	Isoelectric point	References
HAS	66 kDa	~45 mg/mL in human plasma	4.7	[39], [40]
IgG	160 kDa	10mg/mL in human plasma	6.8-6.9	[39], [40]
Fibrinogen	341 kDa	3 mg/mL in human plasma	5.1-5.6	[39], [40]
Transferrin	77 kDa	3 mg/mL in whole human blood	5.35-6.1	[31]
Lysozyme	14 kDa	7-13mg/mL activity In blood serum	11	[36]

For this study, proteins that possess either an acidic or basic isoelectric point have been chosen to compare protein-nanoparticle interactions, The bovine counterpart of HSA, Bovine Serum

Albumin (BSA) and HSA are negatively charged at physiological pH, while LYZ possesses a positive charge under biological conditions. These model proteins will be employed for the analysis of protein-nanoparticle interactions of iron oxide nanoparticles coated with PEGSilane and CMDx polymers.

3 LITERATURE REVIEW

3.1 Protein-nanoparticle interactions

Unpublished work has demonstrated that surface charge in magnetic nanoparticles plays a pivotal role in their internalization into cancerous colon rectal cells (CaCo2) in *in vitro* studies. In figure 4, it can be observed that nanoparticles with low levels of negative surface charge in experiments using Confocal Laser Scanning Microscopy (CLSM) have a lower internalization rate in contrast with particles that possess higher levels of negative surface charge. Certainly, cancer cells do not contain CMDx receptors to promote internalization of CMDx coated magnetic nanoparticles.

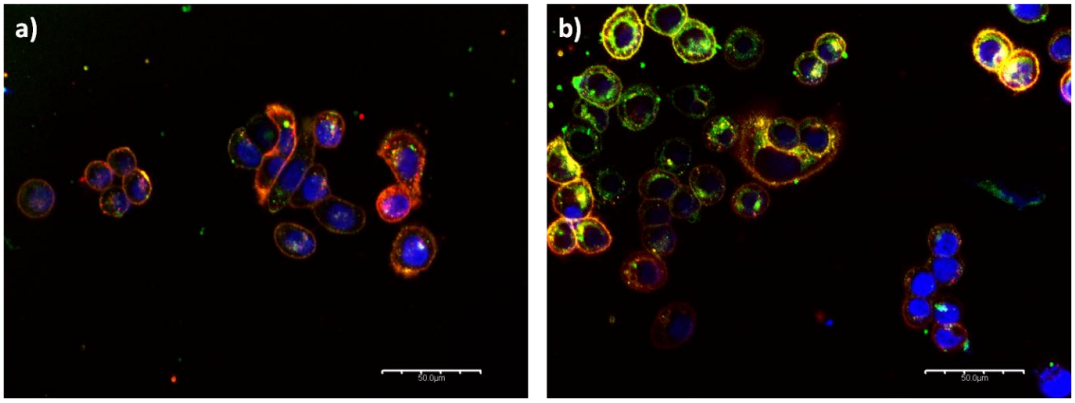

Figure 4. Visualization of green fluorescent a) CMDx 5COOH coated nanoparticles and b) CMDx 23COOH coated nanoparticles, after 1hour of incubation at 37 °C. Cell nuclei were stained with DAPI solution (blue) and cell membranes were stained with DID solution (red).

For this reason, it is hypothesized that these nanoparticles are internalized through protein receptors with the aid of non-specific protein interactions. *In vivo,* the bloodstream and its components have to be taken into account. The physicochemical characteristics of nanoparticles such as composition, shape, particle size, surface charge, and surface hydrophobicity could have an effect on their interaction with plasma proteins and blood components, uptake by macrophages, and consequently influence the biodistribution processes [41], and [42]. Rana et al [43] proposed that the supramolecular interactions between proteins and nanoparticles play a

pivotal role in the applications of nanoparticles *in vivo*. In general, supramolecular chemistry studies the weaker and reversible non-covalent interactions between molecules that include hydrogen bonding, metal coordination, hydrophobic forces, van der Waals forces, and electrostatic effects. Important concepts that have been demonstrated by supramolecular chemistry include molecular self-assembly, folding, and dynamic covalent chemistry, which can be perfectly adapted to nanotechnology science and engineering oriented to biomedical applications [44]. The biophysical properties, such as binding affinity, residence time, binding cooperativity of nanoparticles and common serum proteins have been quantitatively characterized to gain fundamental understanding of the behavior of proteins on nanoparticle surfaces. Many efforts have been directed towards understanding the interactions of nanoparticles with complex protein mixtures such as serum proteins.

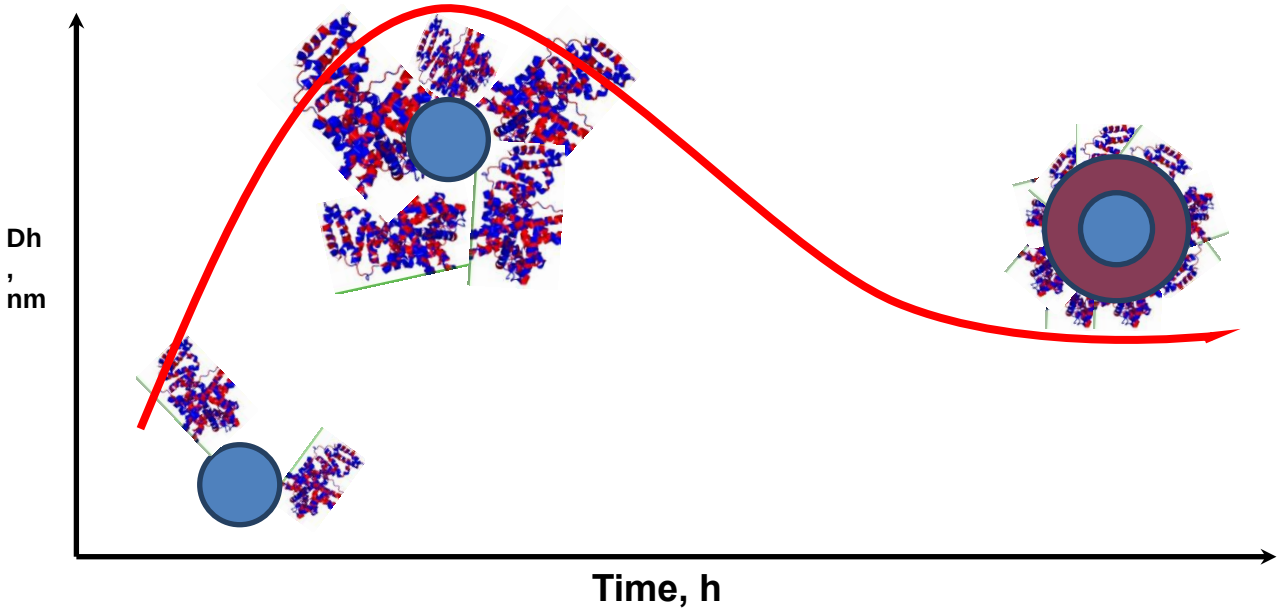

Figure 5. Protein-nanoparticle interactions against time.

A simple model of protein-nanoparticle interactions is proposed in Figure 5. This model shows a clear dependence between nanoparticles hydrodynamic diameter vs. time in presence of proteins. In a biological fluid, like plasma or blood, nanoparticles adsorb proteins, forming the "protein corona". A literature review was performed in order to develop a protocol to evaluate protein-

nanoparticles interactions of PEGSilane coated nanoparticles and CMDx coated nanoparticles for in vivo conditions using centrifugal filter devices. The following table summarizes the literature search:

Table 2. Literature review on protein-particle interactions.

Author	Methods	Summary	Conclusions
Cole et al. [45]	Protein binding study to quantify proteins by spectrophotometric analysis using Bicinchoninic Acid (BCA) assay.	Nanoparticles solution (4.0mgFe/mL) was mixed with phosphatebuffered saline (PBS) and FBS, and incubated for 2 hours at 37 °C. Samples were washed by centrifugation to remove protein excess. Afterwards, 5% sodium dodecyl sulphate (SDS) buffer was added and incubated to remove bound protein for analysis.	PEG-CMDx coated nanoparticles were synthesized to enhance plasma stability and avoid elements of reticuloendothelial system (RES) *in vitro* simulations designed to mimic RES process to predict and understand *in vivo* studies.
Lesniak et al. [46]	The total protein composition of different types of serum was compared and quantified using densitometry.	Polystyrene nanoparticles were incubated in serum for 1 hour at 37 °C and then centrifuged. The supernatant was removed and the nanoparticles's pellet was re-suspended in PBS. Next, the samples were boiled for 5 min to denature proteins, cooled to room temperature and loaded into a gel for electrophoresis.	The amount of adsorbed protein is affected by heat inactivation, and there is a correlation with nanoparticle uptake, because when proteins are adsorbed, particle uptake by cells is decreased.
Bajaj et al [47]	Uptake of BSA-coated Fe_3O_4 nanoparticles in different cell types in absence and presence of serum was performed.	Uptake was quantified using Prussian Blue assay.	The presence of serum plays an important role for *in vitro* applications because serum reduces cellular uptake of magnetic nanoparticles as compared to serum-free conditions.

Table 2. Literature review on protein-particle interactions (continuation).

Author	Methods	Summary	Conclusions
Aggarwal et al [7]	Review paper	Commonly, for protein identification studies, nanoparticles are incubated with an excess of plasma levels because this nanoparticle/protein ratio is more representative of the true biological situation in order to mimic the conditions of bloodstream. The favorite method for isolating nanoparticle-protein complexes is centrifugation.	Comprehension of how proteins bind to nanoparticles, factors that determine affinity, and better ways to manipulate specificity, are all necessary to help get desired biodistribution patterns.
Dobrovolskaia et al [48]	Interaction of colloidal citrate stabilized gold nanoparticles with human plasma. Proteins that bind onto the surfaces were identifying using gel electrophoresis.	This study examines how protein-particle interactions in plasma are affected by size and charge of particles using a combination of DLS, TEM, and AFM techniques in order to elucidate changes after incubation. For do this concentrated particles (0.44mg/mL) were mixed with plasma and incubated for 30 minutes at 37°C. After that, particles were microcentrifuged to remove excess of plasma and protein rehydration buffer was added to isolate proteins.	50 nm nanoparticles bound two times less proteins complex than smaller nanoparticles (20 nm). Study revealed that 69 different proteins bound to the surface of gold nanoparticles, 48 from the 30 nm particles and 21 from the 50 nm particles. Fibrinogen was the most abundantly bound protein.

Table 2. Literature review on protein-particle interactions (continuation).

Author	Methods	Summary	Conclusions
Baier et al [49]	Studies of polystyrene particle uptake in HeLa cells	Particle size and zeta potential measurement were done on the nanoparticles samples after 24 hours incubation in a cell medium with 10 wt% FCS (protein mixture).	The nanoparticles were bigger in size (increase in diameter between 10 and 20 nm) and the size distribution is broader after incubation. Studies with cationic particles shown the presence of aggregates, which might be formed by the negatively charged protein molecules and positively, charged particles.
Owen III, Donald and Peppas, Nicholas [23]	Review paper	The process of opsonization is a biological obstacle to biomedical application of nanoparticles. Opsonin proteins present in the blood serum quickly bind to nanoparticles allowing macrophages to easily recognize and remove these nanoparticles of the system before they can perform their designed function.	It is important to study protein-nanoparticle interactions in order understand the factors that affect stealth materials, long circulating stealth nanoparticles are desirable for nanoparticle applications *in vivo*.
Qin et al [50]	Protein adsorption experiments analyzing UV-vis spectrum supernatants by the UV-vis spectrophotometer.	Magnetic nanoparticles were mixed with different proteins (BSA, lysozyme and γ-globin) in PBS. The mixtures were incubated at 4°C for 5 hours, and separated magnetically.	Proteins were adsorbed observably onto the surface of the naked nanoparticles. The polymer P-(PEGMA) reduces the non-specific proteins adsorption.

Table 2. Literature review on protein-particle interactions (continuation).

Author	Methods	Summary	Conclusions
Meder et al [9]	Quantify protein adsorption on colloidal alumina particles by UV light measurements in the supernatants at 280 nm and using NanoOrange reagent for concentrations above 0.05mg/mL.	For the study the model proteins were lysozyme (LYZ), BSA and trypsin (TRY). Centrifugation at 3,800 g was used to separate unbound proteins.	-NH_2, -COOH, -SO_3H and PO_3H_2 groups in nanoparticle surface has a different impact on the adsorption of LYZ, BSA and TRY. Differences in the hydrophilic/ hydrophobic properties of the nanoparticles surfaces did not obviously affect the among of protein adsorbed.
Lartigue et al [51]	Specific in situ monitoring of interactions between iron oxide nanoparticles and blood plasma by optical birefringence signal induced by an external magnetic field.	Blood plasma protein interactions with iron oxide nanoparticles and the impact on macrophage uptake.	Interactions depend on the concentration of available plasma proteins. At low plasma concentrations (representative of *in vitro* conditions), nanoparticles have a tendency to form clusters triggered by proteins like fibrinogen, whereas at high plasma concentration (closer to physiological situation) other proteins such as apolipoproteins tend to coat and stabilize nanoparticles.

Protein-adsorption research seems to fall into two broad categories, employing two different experimental strategies. The first strategy chooses to quantify only the fraction of adsorbed

protein that remains bound to an adsorbent surface after application of an adsorbent-rinsing protocol [27], [39], and [46]. In pointed contrast, the second strategy defines adsorption as a process that leads to the concentration of the protein within a surface region separating bulk solution from the physical-adsorbent surface, because the interphase must not be perturbed in any way for the measurement of adsorption [39], [51], and [52]. In this work, the experimental protocol used was performed according to literature reviews focusing on procedures based on the first strategy.

For most protein-nanoparticle interactions studies, nanoparticles are incubated with plasma proteins at physiological conditions; methods for particle separation from proteins are subsequently used to remove unbound proteins from nanoparticles. Finally, identification and quantification methods are used to determine binding rates, affinities, and stoichiometry between nanoparticles and serum proteins. A common technique for the identification of the proteins is two-dimensional polyacrylamide gel electrophoresis (2D-PAGE), or for identification of particular proteins, immunoblotting and Western blotting have also been employed [7]. Mahmoudi et al. [52] summarized the most common analytical methods employed to understand the protein corona evolution, thermodynamics and kinetics in nanoparticle-protein complexes, such as spectroscopy methods (including UV/Vis, fluorescence, FTIR, Circular Dichroism, and Nuclear Magnetic Resonance), DLS, Zeta potential, Isothermal Titration Calorimetry (ITC), Differential Centrifugal Sedimentation (DCS), X-ray crystallography and chromatography. All the methods above have advantages and disadvantages, and the accuracy of the results depends on which adsorbed protein fraction is considered for the analysis (Strategy 1 or Strategy 2, as explained above) and the sensitivity of the technique.

One common challenge to arise when quantifying only the fraction of adsorbed protein that remains bound to an adsorbent surface after application of and adsorbent-rinsing procedure is the isolation of the nanoparticle-protein complex from excess proteins without (i) disturbing the complex or (ii) inducing protein binding. The methods used to separate nanoparticles from proteins include centrifugation, gel filtration, membrane-based static microfiltration and

magnetic separation. Centrifugation is regarded as the most suitable method for isolating protein-nanoparticle complexes due to its speed, low cost and ease of use. The spin time and centrifugation velocity to be employed depends on particle and protein morphology and concentration. In contrast to gel filtration, any washing media can be used. Thode et al. [53] demonstrated that using magnetic separation for protein-nanoparticle separation is restricted to particles with high inducible magnetic saturation, in particular, iron oxide nanoparticles (diameters >50 nm). Figure 22 shows a representation of a magnetic separation process adapted from [52].

Figure 6. Representation of magnetic separation technique for protein-nanoparticle separation. Nanoparticle solution before and after separation and rinsing steps.

Even though the centrifugation method is the preferred method for isolating nanoparticle-protein complex, it has many limitations because experimental results can be affected by centrifugation time, pressure, temperature, washing steps, as well as solution volumes used during washing steps while rinsing. As a consequence, a high abundance of proteins may be identified as adsorbed due to insufficient washing; while large protein aggregates that sediment to the bottom of the centrifugation tube may also be falsely identified as interacting proteins.

Since the magnetic nanoparticles used for the studies are colloidally stable in PBS, centrifugation of these particles at high spin velocities of ~21,000g for 1 hour resulted in nanoparticles remaining suspended in the supernatant (see Figure 23), which would cause interference with protein quantification due to the presence of iron in the supernatant. This led us to modify the experimental design based on ultracentrifugation, using Centrifugal Filter Units (CFU) suitable for protein fractionation and protein concentration.

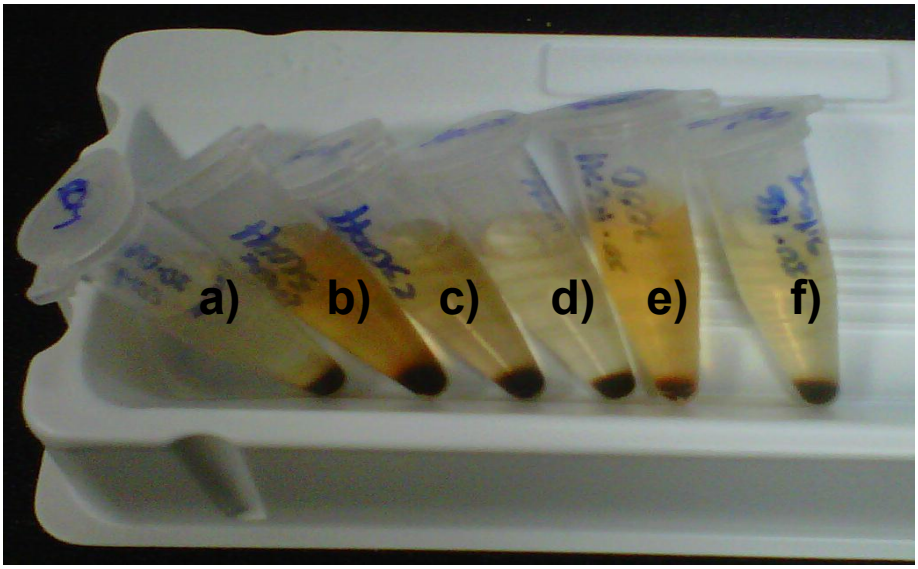

Figure 7. Centrifugation process of CMDx and PEGSilane coated nanoparticles in PBS solution at ~21,000g for 20min at 4°C. a) IO- commercial CMDx, b) IO-5COOH, c) IO-23COOH, d) IO-40COOH, e) IO-PEGSilane2000, and f) IO-PEGSilane5000.

3.2 Centrifugal Filter Units description by manufacturers

Millipore Amicon Centrifugal Filter Units (CFU) have a tangential flow filtration mode (TFF) where the fluid is pumped tangentially along the surface of the membrane, and an applied pressure serves to force a fraction of the fluid through the membrane to the filtrate side. In the outcome, particulates and macromolecules that are too large to pass through the membrane pores are retained on the upstream side. However, in this case the retained components do not build up at the surface of the membrane. Instead, they are swept along by the tangential flow. In addition, for fast sample processing with high recovery in protein concentration applications, Ultracel regenerated cellulose low-binding ultrafiltration membrane combined with a vertical housing is provided in this centrifugal unit (see figure 24). In the literature, TFF is also commonly called cross-flow filtration. However, the term "tangential" is descriptive of the direction of fluid flow relative to the membrane.

Figure 8. Amicon Ultra Centrifugal Devices of varying volumes.

Nanosep® centrifugal devices from Pall Corporation have a normal flow filtration (NFF) mode, where fluid is convected directly toward the membrane under an applied pressure. In this sense, particulates and proteins that are too large to pass through the pores of the membrane accumulate at the membrane surface or in the depth of the filtration media, while smaller molecules pass through to the downstream side. The term "normal" indicates that the fluid flow occurs in the direction normal to the membrane. Each Nanosep® centrifugal device is fabricated of polypropylene and contains low protein-binding Omega™ (modified polyethersulfone)

ultrafiltration membranes (see figure 25), that provide reduced non-specific adsorption and high recovery in protein concentration applications.

Figure 9. Nanosep® centrifugal devices from Pall Corporation in a selection of different molecular weight cutoff.

4 OBJECTIVE

The main aim of this work is to study how the behavior of biocompatible nanoparticles with varying surface charge and different polymeric coatings is affected in the presence of proteins that simulate *in vivo* conditions. The effects of (i) CMDx surface- coated nanoparticles with different degrees of carboxylic acid group substitution, and (ii) the molecular weight of PEGSilane coated nanoparticles on protein-nanoparticle interactions have not been studied in detail. In addition, Centrifugal Filter Devices (CFD) are powerful tools to separate unbound proteins from protein-nanoparticle complexes, useful in the development of a protein-nanoparticle interaction study protocol. For all the reasons above the study of the effects of nanoparticle surface charge on protein interactions using CFDs and magnetic nanoparticles with various surface properties was proposed. This information will give a better understanding of how nanoparticle surface chemistry can influence behavior of *in vivo* experiments. The results of this study will be used to complement the understanding of biodistribution and pharmacokinetic studies performed recently in mice and rats.

To accomplish these objectives, several tasks needed to be performed:

- Synthesis and characterization of colloidally stable PEGSilane coated iron oxide nanoparticles using the co-precipitation method using PEG of different molecular weights.
- Synthesis and characterization of colloidally stable CMDx coated particles with different degrees of carboxylic acid group substitution using the co-precipitation method.
- Development of a protocol to study protein adsorption on iron oxide nanoparticles using a phosphate buffered saline wash protocol, the bicinchoninic acid assay (BCA), and mass balance calculations.

5 EXPERIMENTAL AND METHODS

5.1 PEGSilane coated nanoparticles

5.1.1 Materials

Poly(ethylene glycol) methyl ether (mPEG, 2000, and 5000 g/mol), chromium trioxide, acetic acid, and sulfuric acid were purchased from Sigma Aldrich and used as received. Toluene and 3-aminopropyl triethoxysilane (APS) were purchased from TCI America and used as received.

5.1.2 Synthesis of PEGSilane coated nanoparticles

Iron oxide nanoparticles (Fe_3O_4) with wide size distribution were obtained following the procedure proposed by Herrera et al [22] by the co-precipitation method. Briefly, coprecipitation of Fe^{+3} (iron (III) chloride hexahydrate), and Fe^{+2} (iron (II) chloride tetrahydrate) salts took place with a Fe^{+3}/Fe^{+2} ratio equal to 2.73 under a N_2 atmosphere at 80 °C for 1 hour. After that, particles were centrifuged for 10 min at 1500 rpm and decanted from the supernatant using a magnet. Iron oxide particles were then peptized with tetrametylammoniun hydroxide ($(CH_3)_4NOH$) via centrifugation for 10 min at 1500 rpm. Finally, the resulting black sticky paste was placed in the vacuum oven at 60 °C overnight.

In order to incorporate oleic acid molecules onto the magnetic cores, an adsorption reaction at 80°C for 1 hour with 2.27% v/v. of oleic acid in water was performed. The colloid was supersonicated (20% power) for 90 seconds in order to break aggregates in solution. After that, particles were suspended for 20 min using lower sonication, then the oleic acid was added to the solution and left to react. To remove the free oleic acid, nanoparticles were washed once with ethanol (1:3) via centrifugation at 7500 rpm for 15 min. Magnetic separation was used to discard the supernatant and collect the particles.

Mono-methoxy PEG (mPEG) of 2000 and 5000 molecular weight were converted to oxidized PEG (mPEG-COOH) using Jones reagent, a strong oxidizing agent which converts terminal hydroxyl group in mPEG polymers to carboxylic acids. For this, 0.05 mol of mPEG in 400 mL of acetone were dissolved followed by the addition of 17 mL of Jones reagent. The mixture was stirred at room temperature for 24 hours and quenched by addition of 5 mL of isopropyl alcohol. To remove chromium salt by-products of the reaction, charcoal was added to the mixture (10% w/w with respect to polymer mass). Afterwards, the mixture was vacuum- filtered until a clear acetone solution was obtained. Finally, this solution was concentrated to a viscous liquid using a rotary-evaporator and then dried in the vacuum oven at 60 °C overnight [54].

To synthesize PEGSilane polymers, mPEG-COOH was reacted with 3-aminopropyl triethoxysilane in a 1:1 molar ratio under nitrogen atmosphere at 180 °C for 2 hours. A brown paste was obtained, and was stored in the desiccator. Finally, to prepare PEGSilane coated nanoparticles, a ligand exchange reaction was followed. Fundamentally, oleic acid molecules on the magnetic cores were replaced by PEG-Silane polymers of different molecular weights in toluene (~ 5.55 mg polymer/mL) using acetic acid as a catalytic agent following the procedure proposed by Barrera et al.[17].

5.1.3 Characterization of PEGSilane coated nanoparticles

Biocompatible iron oxide magnetic nanoparticles coated with PEG were prepared by replacing oleic acid with a biocompatible synthesized PEGSilane to provide an easy and effective method for chemical coating. In order to obtain colloidally stable iron oxide nanoparticles with potential uses in biomedical applications the following characterization procedures were performed:

5.1.3.1 Infrared spectroscopy

Infrared spectroscopy in a Varian 800 Transform Infrared (FTIR) equipment was used to study changes in functional groups obtained through the synthesis of peptized iron oxide, coating of nanoparticles with oleic acid, the presence of mPEG-COOH and PEG-Silane polymers, and the coating of nanoparticles with PEG-Silane. Powder samples were placed on a Pike attenuated total reflectance (ATR) stage with ZnSe window. The results are presented as plot transmittance (adimensional units) vs. wavenumber (cm^{-1}).

5.1.3.2 Transmission Electron Microscopy (TEM)

Particles were suspended in a concentration of 1 mg/mL of solvents such a water (IO-Peptized, IO-PEGSilane) and chloroform for oleic acid coated nanoparticles, placed in copper grids and dried in a vacuum oven for 30 min. A JEOL 1200EX Transmission Electron Microscope (TEM) equipment was used to take pictures in order to analyze size and distribution of magnetic cores.

The volume weighted mean diameter (D_{pgv}) and geometric deviation ($\ln\sigma_g$) of the nanoparticles was acquired by determining the diameter for at least 50 particles (depending on picture quality) using the image analysis program ImageJ (Distributed by NIH) and fitting to a log-normal sized distribution that corresponded to the follow equation reported by Lopez et al [55]:

$$n(D_p) = \frac{1}{\sqrt{2\pi} D_p \ln \sigma_g} \exp\left(- \frac{\ln\left(\frac{D_p}{D_{pgv}} \right)}{2 \ln^2 (\sigma_g)} \right) \qquad (1)$$

5.1.3.3 Dynamic Light Scattering and Zeta Potential measurements

A Brookhaven Instruments BI-90 Plus Particle Size and Zeta Potential Analyzer was used to determine the hydrodynamic diameter size and surface charge of the particles for each synthesis step. The hydrodynamic size of peptized nanoparticles, oleic acid- coated nanoparticles, and nanoparticles coated with PEGSilane of different molecular weights particles was studied suspending particles (1mg/mL) in dimethyl sulfo oxide (DMSO), hexane, and water, respectively. For DLS measurement the data is interpreted using intensity, volume, surface area and number functions of the equipment, which provides a histogram of particle size D and their corresponding relative intensity Gd. Results were summarized in lognormal distribution graphs.

In order to study colloidal stability against pH, zeta potential and DLS measurements were performed at 25°C, 0.67mg particle concentration/mL, and 100nM KNO3 in deionized distillated water, with pH adjusted from 2 to 12 by adding of 0.1 M KOH and 0.1 M HNO_3. For these studies average hydrodynamic diameter Dh and standard deviations σ will be determined from (2) using volume data distributions of the equipment:

$$D_h = \frac{\sum DG_d}{\sum G_d}, \sigma = \left[\frac{\sum \left(G_d \left(D_h - D \right)^2 \right)}{\sum G_d} \right]^{0.5} \quad (2)$$

5.1.3.4 Thermogravimetric Analysis (TGA)

Mettler Toledo STARe TGA/DSC1 Thermogravimetric Analyzer equipment was used to estimate the amount of PEGSilane attached onto the magnetic cores. Samples were dried at 115 °C in order to remove adsorbed water and solvent traces. A temperature ramp from 25°C to 800°C was used, with a heating rate of 10°C/min in air atmosphere. Samples were analyzed in triplicate to obtain an average of the remnant weight loss.

5.1.3.5 Magnetic properties and Specific Adsorption Rate (SAR) measurements

A Quantum Design MPMS XL-7 SQUID (Superconducting Quantum Interference Device) equipment was used in order to obtain results for magnetization as a function of applied field at 300K obtained for dry powders of magnetic nanoparticles. Magnetization was normalized with respect to Fe_3O_4 mass in the samples, determined by thermogravimetric analysis, to obtain magnetization per unit mass. The SQUID data was fitted using a non-linear regression to a model consisting of the Langevin-Chantrel function taking into account a lognormal particle size distribution to estimate the volume mean magnetic diameter and the geometric deviation of the distribution [42].

The energy dissipation due to rotational relaxations of magnetic particles dispersed in a liquid matrix in an oscillating magnetic field was quantified by SAR and estimated from calorimetric measurements using:

$$SAR = \frac{\sum C_i m_i}{m_{Fe}} \left(\frac{dT}{dt} \right)_{t \to 0} \quad (3)$$

where C_i and m_i are the heat capacity and mass of each component of a suspension in water (0.6mg of magnetic core/mL). The heat capacity could be approximated using the heat capacity of water (4.1813 J/(g•K)). According to 3, mFe is the amount of iron present in the sample and dT/dt is the initial slope of the sample temperature as a function of time during an experiment where nanoparticles suspended in water are put into an induction coil connected to an RDO Induction HFI-3kW induction heater at different magnetic fields. Samples were prepared in triplicate in order to estimate an average of SAR measurements [57]. Heating of the PEGSilane2000 and PEGSilane5000 coated nanoparticles was studied by performing SAR measurements on 0.6 mg magnetic core per mL in water using oscillating magnetic field between 16 kA/m to 47.5 kA/m at 233 kHz.

5.2 CMDx coated nanoparticles

Biocompatible iron oxide magnetic nanoparticles coated with CMDx with different degrees of substitution of carboxylic acid were prepared via EDC/NHS chemistry in order to attach covalently CMDx polymers onto the surface of APS coated nanoparticles such was reported as Herrera et al [22].

5.2.1 Synthesis of CMDx with different degrees of substitution

For the purpose of these studies, CMDx polymers with 5 COOH, 23 COOH, and 40 COOH degrees of substitution of carboxylic acid per dextran chain were prepared following a previous procedure described by Ayala in her MS thesis [58]. Modified polymers were prepared by carboxymethylation reaction of Dextran obtained from *Leuconostoc mesenteroides* by reacting monochloro acetic acid in the presence of sodium hydroxide at 70 °C for 1 hour. The degree of carboxymethylation was controlled by adjusting sodium hydroxide concentration. In general, 20 g of dextran were dissolved in 100 ml of distilled water. Sodium hydroxide (NaOH) was dissolved in 34 ml of distilled water, for a final concentration of 1M, 2M or 3M (depending of the desired degree of substitution of -COOH groups per dextran chain). The solutions were cooled in an ice bath to 4 ºC. Afterwards, NaOH was added drop wise to the dextran solution slowly. Then, 29.16 g of solid monochloro acetic acid was added and dissolved using a small rotor. After the reaction, the mixture was neutralized with acetic acid before reaching room temperature. The product was precipitated with ethanol overnight. The solid paste was recovered, suspended in water (20 mL) and dialyzed until a conductivity of $\leq$ 10 μS/cm was obtained from the dialysis water. Finally, the CMDx was concentrated using a Brinkmann RE 121 rotary evaporator and dried at 60 ºC. The dried sample was powdered and stored at 4°C.

5.2.2 Synthesis of CMDx coated nanoparticles with different degrees of substitution of carboxylic groups

Magnetic nanoparticles were synthesized by the coprecipitation method and peptized with tetramethylammoniun hydroxide. Peptized nanoparticles were functionalized with APS to graft functional amine groups (-NH2) onto the nanoparticles surface. For this, peptized nanoparticles were suspended in DMSO, 10 mL APS, 1.25 mL water, and 100 μL acetic acid.

The reaction mixture was mechanically stirred at 150 rpm during 72 hours at room temperature. Afterwards, nanoparticles were washed four times with ethanol, and dried at room temperature to obtain a layer of black solid APS coated nanoparticles (IO-APS). IO-APS nanoparticles were functionalized with CMDx via EDC/NHS chemistry. Carboxylic groups (-COOH) present in the CMDx reacted with NHS in presence of EDC, resulting in a semi-stable ester, which can then be reacted with primary amines present in the IO-APS nanoparticles, forming a covalent bond. This was carried out dissolving 4 g of CMDx in 40 mL deionized water (pH 4.5-5), with 100 mg of EDC and 60 mg of NHS. Finally the CMDx solution was mixed with the IO-APS solution (0.4 g IO-APS per 40 mL of deionized at the same pH). The reaction mixture was mechanically stirred at 150 rpm during 36 hours at room temperature. Finally, CMDx coated nanoparticles were washed three times with ethanol (1:3) by centrifugation at 7500 rpm for 15 min, and dried at 60 °C in the vacuum oven. The nanoparticles were stored at 4 °C for further experiments. This procedure was followed for each of the CMDx synthesized (5 COOH, 23 COOH, and 40 COOH).

5.2.3 Characterization of CMDx coated nanoparticles with different degrees of substitution

The same characterization techniques used to analyze PEGSilane coated nanoparticles were used to characterize CMDx coated nanoparticles. Particle size was measured using a Zeiss 922 TEM. A Brookhaven Instruments BI-90 Plus Particle Size Analyzer and Zeta Potential Analyzer were used to determine the hydrodynamic size and zeta potential of the particles. Magnetic properties of magnetic nanoparticles were studied using a Quantum Design MPMS XL-7 SQUID Magnetometer. The amount of bound CMDx was analyzed by thermogravimetric analysis under an air atmosphere.

5.3 Colloidal stability studies in biological buffers

The colloidal stability of PEG-Silane coated nanoparticles was studied through a wide variety of experiments. These experiments included hydrodynamic diameter measurements in different biologically relevant media, such as: dulbecco's modified eagle's medium- high glucose (DMEM), minimum essential medium (EMEM), RPMI-1640 Medium, phosphate buffered saline (PBS), hanks' balanced salts (HBSS), HEPES ((4-(2-hydroxyethyl)-1-piperazineethanesulfonic acid)), and deionized distillated water (DDW) at 25°C. Also, the formulations were analyzed at 37 °C, and 47°C, temperatures that model the biological environment and magnetic fluid hyperthermia treatment conditions. Particles were autoclaved at 121 °C and resuspended in the biological buffer at 1mg of particle total per milliliter of solution before starting the measurements. Time storage effect of the previous formulations was tested from 1 h to 72 hours. At 47°C, time storage effect was only tested for 1 hour because this is the range of time usually employed for MFH. he effect of the temperature was important because in prior experiments with PEGSilane5000 coated nanoparticles, storage at 4°C produced a slight precipitate, but particles stored at room temperature did not present the same behavior. They still retained a clear colloidal appearance.

5.4 Protein-nanoparticle interactions studies

For protein-nanoparticle interaction studies, nanoparticles synthesized and characterized previously were used: nanoparticles coated with CMDx with different degrees of COO- substitution and PEGSilane- coated nanoparticles. CMDx is a polysaccharide, which was altered to include varying degrees of COO-, thus formulating dextran chains with various degrees of charge. PEGSilane is a polymer of ethylene oxide. The hypothesis of this study is that nanoparticles coated with PEGSilane polymers and CMDx 5COOH polymer should show minimal interactions between proteins and nanoparticle surface, because they possess a near neutral surface charge at physiological pH and less reactive groups than the surface of nanoparticles coated with CMDx 23 COOH and CMDx 40 COOH polymers. Reactive groups in CMDx coated nanoparticles correspond to –COOH groups. PEGSilane coated nanoparticles can include $–NH_2$ groups due to unreacted APS.

For this approach, each nanoparticle was incubated with either BSA or LYZ for 2 hours at 37°C degrees in PBS (pH 7.4). Protein-nanoparticle solutions were centrifuged at 1500g for 20min at room temperature (~25°C). The centrifugation steps were carried out in Amicon Ultra 100K 0.5mL centrifugal filters, with the aim of distinguishing between proteins strongly bonded to nanoparticles from weakly- interacting or unbound proteins. Particles with strongly bonded proteins are expected to remain in the membrane, and weakly interacting or unbound proteins are expected to pass through the membrane as a filtrate. Three subsequent wash steps with PBS were included to remove remaining unbound proteins. The protein concentration in solutions was determined spectrophotometrically at a wavelength of 562 nm by BCA assay.

The results suggested that protein was strongly bound to the nanoparticle surface. However, it was discovered that there were several operation conditions that could affect retention or filtration of proteins during centrifugation (CFU cutoff, time, spin rate, temperature, and protein concentration).

5.5 Protein and particle sedimentation studies

These studies were performed at high spin velocity centrifugation in eppendorf tubes with the objective to validate protein sedimentation instead of protein adsorption in PEGSilane and CMDx coated nanoparticles. Firstly, protein solutions at different concentrations, 1mg/mL, 10 mg/mL, and 60mg/mL were prepared in PBS solution. Centrifugation of 1mL of solutions at ~21,000g for 80min at 4°C was realized for all samples. Secondly, protein concentrations in the stock solutions and supernatants were quantified by BCA assay.

For sedimentation studies of magnetic nanoparticles 1mgcore/mL solutions in PBS were prepared, and 1mL of solutions were centrifuged at ~21,000g for 80min at 4°C. Iron content in stock solutions and supernatants was estimated using a colorimetric assay via hydroxylamine as the reducing agent and 1,10-phenanthroline as the complexing agent. Details of 1,10-phenanthroline protocol for iron determination can be found in the appendix section.

6 RESULTS AND DISCUSSION

6.1 PEGSilane coated nanoparticles

6.1.1 Infrared spectroscopy

The FTIR spectra of peptized, oleic acid and PEG-Silane coated iron oxide nanoparticles are presented in Figure 6. The characteristics peaks of Fe-O bonding can be observed partially near the 586cm^{-1} wavenumber for all the plots. For peptized nanoparticles a broad peak around 3179 cm^{-1} corresponded to the oxidized magnetic surface FeO-H [18].

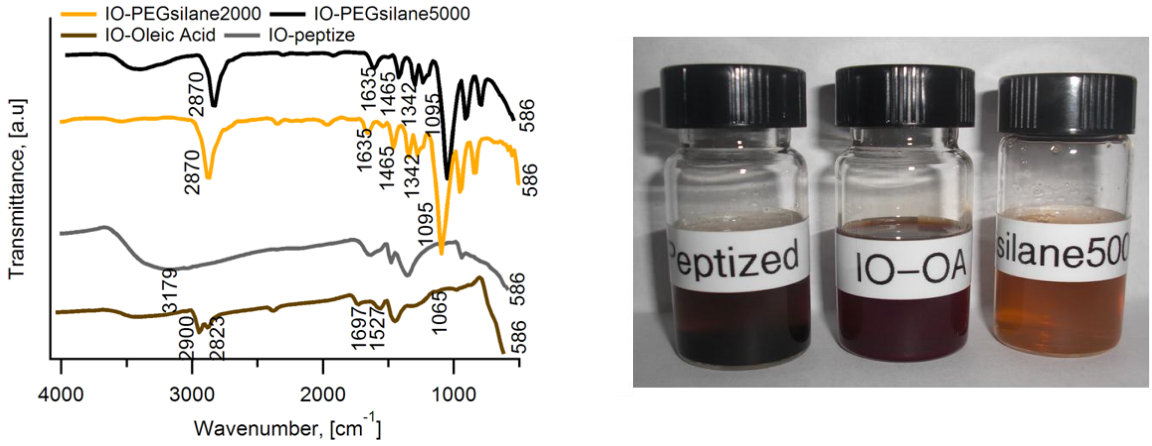

Figure 10. FTIR measurements for PEG-Silane coated nanoparticles

In concordance with Zhang et al [34], oleic acid coated nanoparticles showed relevant vibration bands at 1681 cm-1 and 1543 cm-1, characteristic of asymmetric and symmetric COO- vibration of the chelating bidentate contact between oleic acid and Fe atoms on the surface of the particles. Additionally, two bands at 2900 and 2823 cm-1 were attributed to the asymmetric CH_2 stretch and the symmetric CH_2 stretch, in oleic acid respectively. An adsorption peak at 1065 cm-1 arises from C–O single bond stretching. These peaks confirm, as described in literature, that oleic acid molecules were chemisorbed onto the Fe_3O_4 surface. In the FTIR spectra of PEGSilane coated nanoparticles, the Si-O-Fe and Fe-OH peaks were detected between 800-900

cm^{-1}. The peak at 1095 cm^{-1} is characteristic of –COC vibrations from the ether group in PEGSilane. Also, a strong band at 2780 cm^{-1} was attributed to C-H stretching vibrations. A band appeared at 1635 cm^{-1}, characteristic of the –C(=O)–NH vibration in PEGSilane [18], and [59].

6.1.2 Transmission Electron Microscopy (TEM)

Transmission Electron Microscopy (TEM) images in figure 7 showed that particles have a wide size distribution and are less agglomerated after exchange of OA to PEG-Silane of various molecular weights. Note that although particles are seen in clusters there is space between them due to the grafted PEG, which is not visible through TEM.

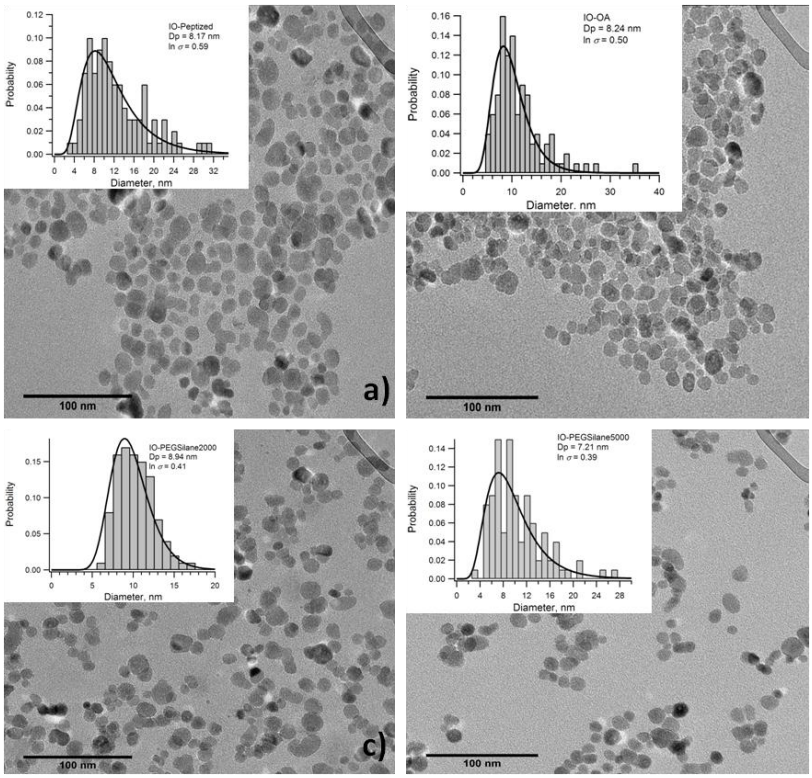

Figure 11. TEM images of iron oxide nanoparticles: a) peptized, b) covered with OA, c) IO-PEGSilane2000 particles and d) IO-PEGSilane5000 particles.

Volume mean diameter D_{pg} of 8.17 nm and a geometric deviation ln σ_g of 0.59 were obtained for IO-Peptized nanoparticles. For IO-OA, a Dpg of 8.24 nm and a geometric deviation lnσ_g of 0.50 were obtained, and by diameter differences it can be inferred that a thin layer of oleic acid was successfully attached onto the magnetic core. Moreover, volume mean diameter D_{pg} increased after ligand exchange of OA molecules with PEGSilane2000 (D_{pg} = 8.94 nm; lnσ_g = 0.41) but decreased with PEGSilane5000 (D_{pg} = 7.21 nm; lnσ_g = 0.39). This behavior probably is due to breaking of magnetic aggregates after ligand exchange process.

6.1.3 Dynamic Light Scattering and Zeta Potential measurements

DLS results for PEGSilane coated nanoparticles per each process step are presented in figures 8 to figure 11. Samples were suspended and filtered showing commonly bimodal populations, because the co-precipitation synthesis method generates polydisperse and aggregate particles.

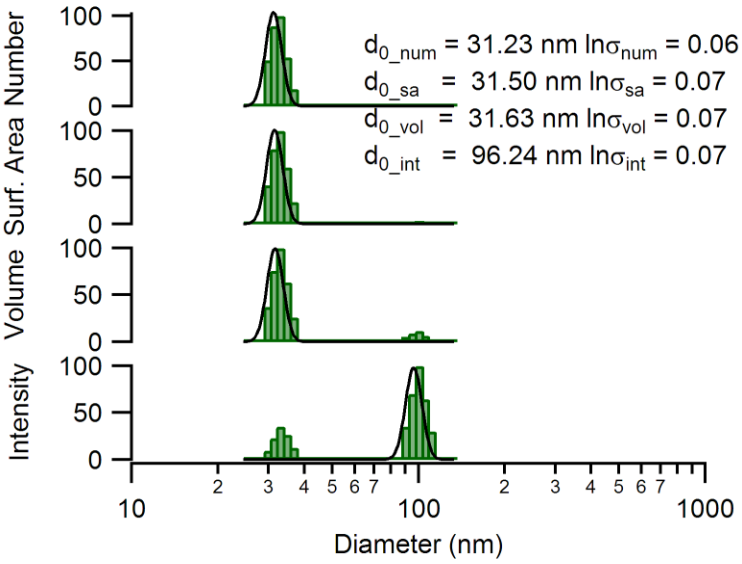

Figure 12. DLS of IO-peptized nanoparticles in DMSO (Solution filtered in a 0.1µm filter)

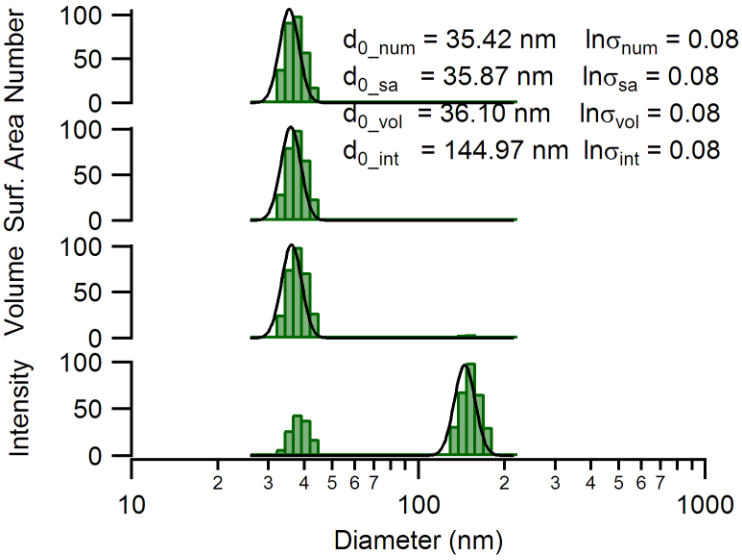

Figure 13. DLS measurements of OA coated nanoparticles in hexane (filtered solution 0.1μm filter)

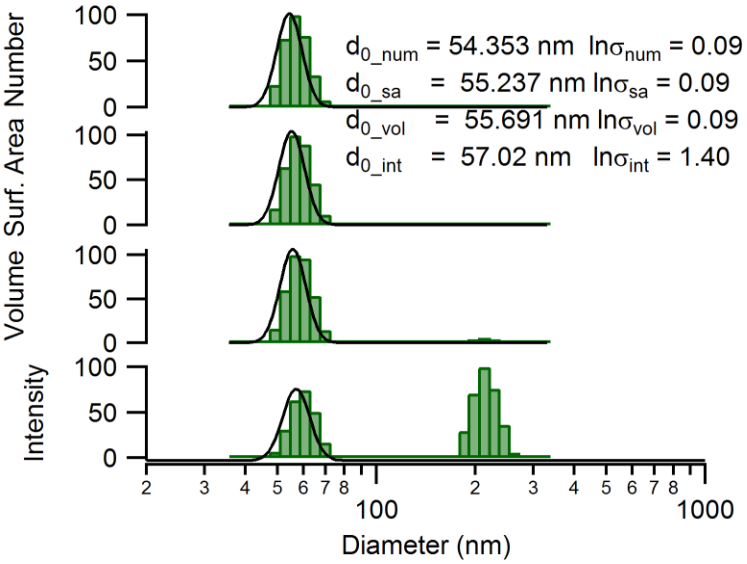

Figure 14. DLS measurements PEGSilane 2000 coated nanoparticles in water (Solution filtered in a 0.2μm filter)

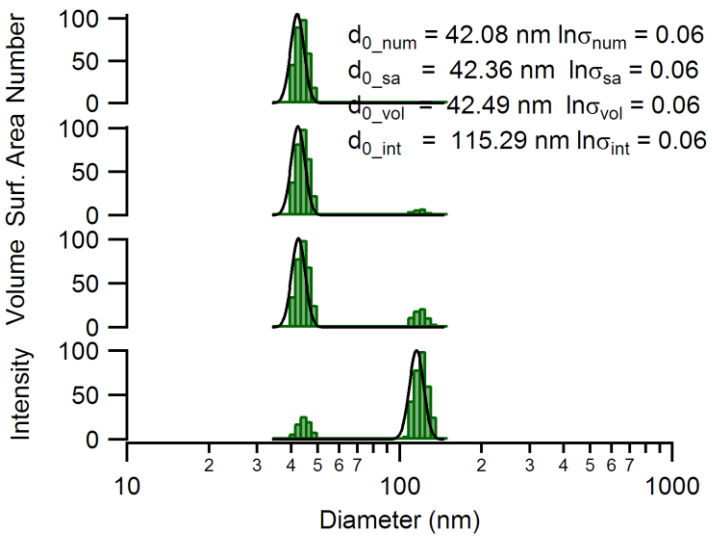

Figure 15. DLS measurements PEGSilane 5000 coated nanoparticles in water (Solution filtered in a 0.2μm filter)

The DLS results demonstrate that peptized particles consist primarily of a distribution of volume with a mean size of 32 nm. OA coated nanoparticles consisted of a distribution with a mean size of 36 nm. IO-PEGSilane2000 and IO-PEGSilane5000 nanoparticles had a distribution of volume with a mean size of 56 nm and 42 nm correspondingly. No visible aggregation was observed in the bottom of the solutions after 24 hours. This indicates that the particles are stable for at least 24 hours.

The tendency of DLS and zeta potential results in water at pH≈7.4 and room temperature are shown in figure 12 with dashed lines. Mainly, particles had a distribution with mean size of 52.78 nm (σ= 3.48 nm) and 2.05μm (σ = 0.11 μm), for PEGSilane2000 and PEGSilane5000 coated nanoparticles respectively. PEGSilane5000 sample showed significant aggregation in contrast with PEGSilane2000 when pH was higher than 4.6. PEGSilane2000 coated nanoparticles were stable against all pH conditions measured. At low pH values PEGSilane5000 particles were stable, but at basic pH values particles had visible aggregation and the DLS measurements were not reliable. It is possible that particles precipitated due to loss of electrostatic stabilization. This is attributed to the fact that at physiological pH, PEGSilane2000

particles achieved a neutral surface due to the poor availability of amine groups of unreacted APS that suggests the presence of a strong steric stabilization offered by PEGSilane2000 polymer chains. In contrast, PEGSilane5000 particles present a positive charge at physiological pH due to the protonation of amine groups of unreacted APS.

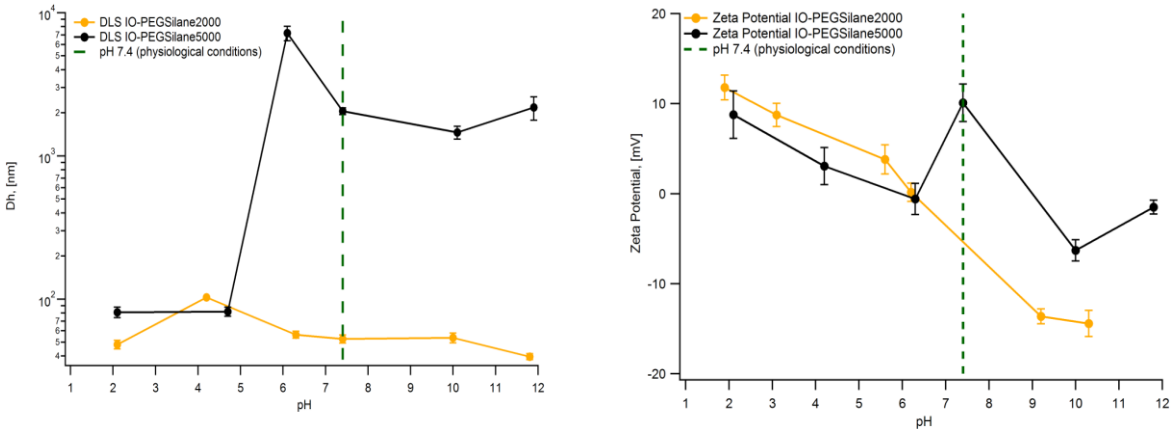

Figure 16. DLS and Zeta potential measurements of PEGSilane coated nanoparticles.

To understand PEGSilane5000 particle aggregation at pH higher than 5, it is hypothesized that polymer depletion effect leads to an unbalanced osmotic pressure, pushing the large particles together, which results in an effective attraction between large particles and subsequent particle precipitation. This is suggested by the lower content of magnetic core present in PEGSilane5000 nanoparticles in contrast to PEGSilane2000 nanoparticles (reported in table 3). The polymer excess is probably due to an inefficient washing step of unreacted PEGSilane. The possibility of an inefficient covering process with PEGSilane5000 onto the surface of magnetic cores can be another important fact. Also, it is interesting to take into account that the depletion effect in PEGSilane particle systems is complicated because there is a mixture of large clusters that affect colloidal stability considerably if successful coating is not performed. Coating of nanoparticles by PEGSilane is strongly dependent on the size distribution of magnetic cores; in contrast, previous studies using PEGSilane ligand exchange employing monodisperse nanoparticles were successful [17].

6.1.4 Thermogravimetric Analysis (TGA)

In Figure 13, the weight loss behavior for PEGSilane coated nanoparticles can be observed. Peptized nanoparticles show two inflexion points due to tetramethylammoniun hydroxide traces and adsorbed water. A mass loss of about 22.19% at 188 ◦C was found for OA coated nanoparticles, attributed to the degradation of oleic acid. PEGsilane5000 coated nanoparticles presented a high loss of organic compounds in contrast with PEGSilane2000 coated nanoparticles. This could explain the poor colloidal stability of PEGSilane5000 coated nanoparticles at pH higher than 4.6, because of the availability of high levels of unreacted amine groups in a vast polymer coating. It is probable that large polymer coatings with positive surface charges saturated steric stabilizations in these particles. For these reasons, it can be speculated that nanoparticles coated with PEG around 2000 Mw or less are typically reported in literature. One example is that Larsen et al [18] successfully performed a ligand exchange reaction with commercially available PEGSilane with a molecular weight distribution of 596-725 Da.

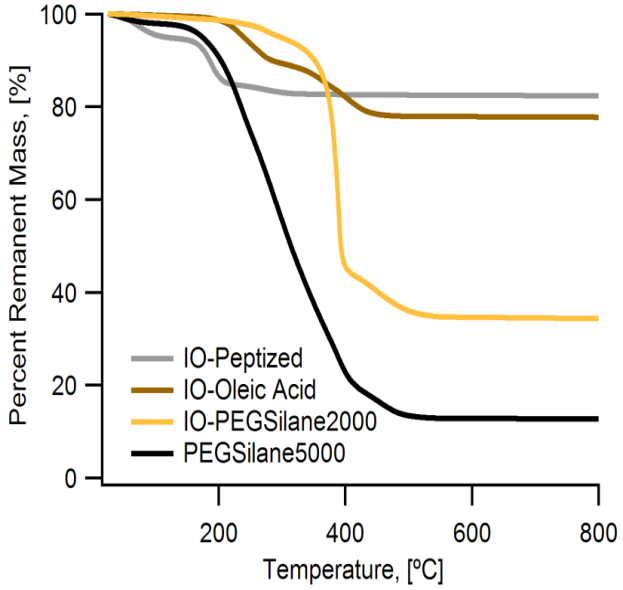

Figure 17. Remanent weight loss of peptized, oleic acid, and PEGSilane coated magnetic nanoparticles.

TGA measurements were performed to estimate percent of magnetic core in the modified nanoparticles. The results are summarized in Table 3.

Table 3. TGA measurements to determine percent of magnetic core in PEGSilane coated nanoparticles.

Particles	Average, % of magnetic core	Std Deviation, % of magnetic core
IO-peptized	82.42	1.52
IO-OA	77.81	0.24
IO-PEGSilane2000	36.10	1.62
IO-PEGSilane5000	12.77	1.79

Values presented in table 3 indicate that 65.60% of the mass corresponds to PEG-Silane2000, and the 34.40% represents iron oxide magnetic core. For PEGSilane 5000, 83.27% of the mass corresponds to PEGSilane5000, and the 12.77% represents iron oxide magnetic core. PEGSilane 2000 particles are more concentrated in terms of magnetic core.

6.1.5 Magnetic properties and Specific Adsorption Rate (SAR) measurements

Measured temperature-time curves for PEGSilane2000 are shown in Figure 14 with calculated SAR values for PEGSilane2000. An appreciable temperature rise is observed (~15°C). The calculated SAR values under the conditions of the experiments are no more than 75 W/g. For all magnetic fields applied, an increase of SAR values was observed.

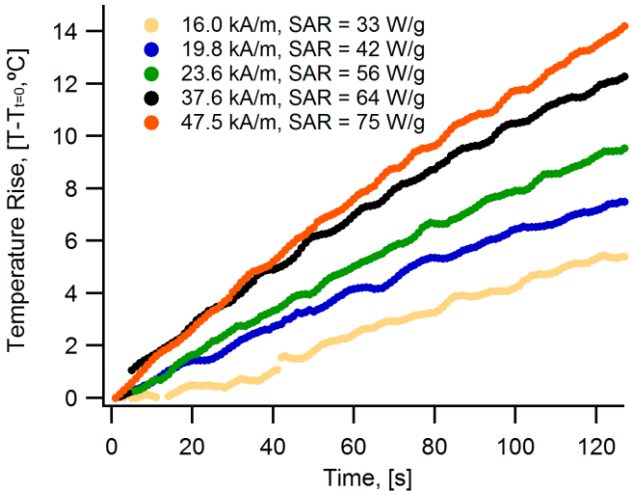

Figure 18. Specific absorption rate (SAR) measurements of PEGSilane2000 coated nanoparticles at different magnetic field amplitudes.

For PEGSilane5000, measured temperature-time curves are shown in Figure 15 with calculated SAR values. No appreciable temperature rise was observed. The calculated SAR values under the conditions of the experiments are no more than 100 W/g. At 37.6 and 47.5 kA/m, significant differences in SAR measurements (88 and 89 W/g_{Fe3O4}) are not observed.

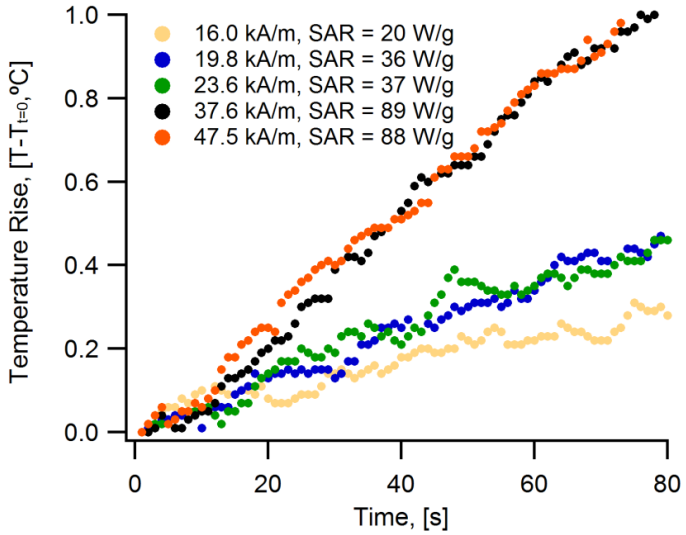

Figure 19. Specific absorption rate (SAR) measurements of PEGSilane5000 coated nanoparticles at different magnetic field amplitudes.

In general, PEGSilane2000 coated nanoparticles have a higher percent of magnetic core than PEGSilane5000 coated nanoparticles (~36%), for this reason the heating is higher.

Figure 16 shows that all samples were superparamagnetic (no hysteresis). Magnetization losses were observable in the studied magnetic field for oleic acid coated nanoparticles and PEGSilane particles, in contrast with peptized nanoparticles. Equilibrium magnetization measurements at 300K for PEGSilane coated iron oxide nanoparticles indicate that the molecular weight of the grafted PEGSilane has an effect on the magnetic properties of the nanoparticles, with saturation magnetization of 64 Am^2/kg and 48 Am^2/kg for PEGSilane2000 and PEGSilane5000 respectively, which is a reduction of about 25% of magnetization. This is consistent with the observed saturation magnetizations, which are lower than the bulk values for iron oxides (~80 Am^2/kg for maghemite and ~90 Am^2/kg for magnetite) [60] .

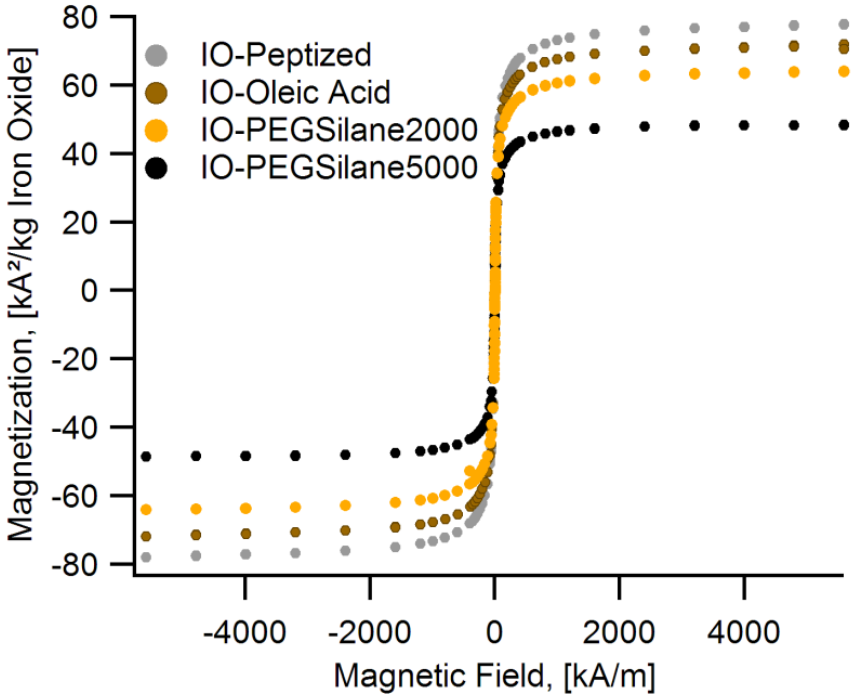

Figure 20. Saturation magnetization at 300K of peptized, oleic acid and PEGSilane coated nanoparticles.

Reproducibility in the preparation of PEGSilane coated nanoparticles was tested with five batches of preparation (data not shown) using DLS and TGA measurements. Generally, reproducibility and enhancement in the preparation of PEGSilane5000 was not obtained after several trials. However, reproducibility in PEGSilane2000 results was successfully obtained. After validation of colloidal stability in biological buffers, testing of PEGSilane2000 nanoparticles's citotoxicity *in vitro* is recommended in order to confirm the potential uses of these particles in cancer treatments such as Magnetic Fluid Hyperthermia (MFH).

The ligand exchange for these particles using PEGSilane5000 was problematic. Irreproducible results were likely due to the presence of unreacted amine groups; the high molecular weight of PEG did not seem to contribute to nanoparticle steric stabilization. PEGSilane2000 coated co-precipitation nanoparticles of 52.78 ± 3.48 nm in water at physiological pH were obtained with a straightforward and reproducible method. IO-PEGSilane2000 nanoparticles have a stable hydrodynamic diameter across a range of pH at room temperature in water. PEG-Silane2000 coated nanoparticles with a saturation magnetization of 64emu/g and a magnetic core of 36.40% are suitable for MFH applications.

6.2 CMDx coated nanoparticles

6.2.1 Transmission Electron Microscopy (TEM)

Figure 17 shows a representative image of the synthesized nanoparticles, from which observe slight aggregation of the magnetic nanoparticles into small clusters can be observed. The IO CMDx 5COOH nanoparticles exhibited a number mean diameter of 10.92 nm with a geometric deviation ln σ_g of 0.65. For IO CMDx 23COOH D_{pg} of 6.84 nm and a geometric deviation ln σg of 0.51 were obtained. In IO CMDx 40 COOH particles, volume mean diameter D_{pg} was 9.42 nm with a geometric deviation of ln σ_g of 0.26.

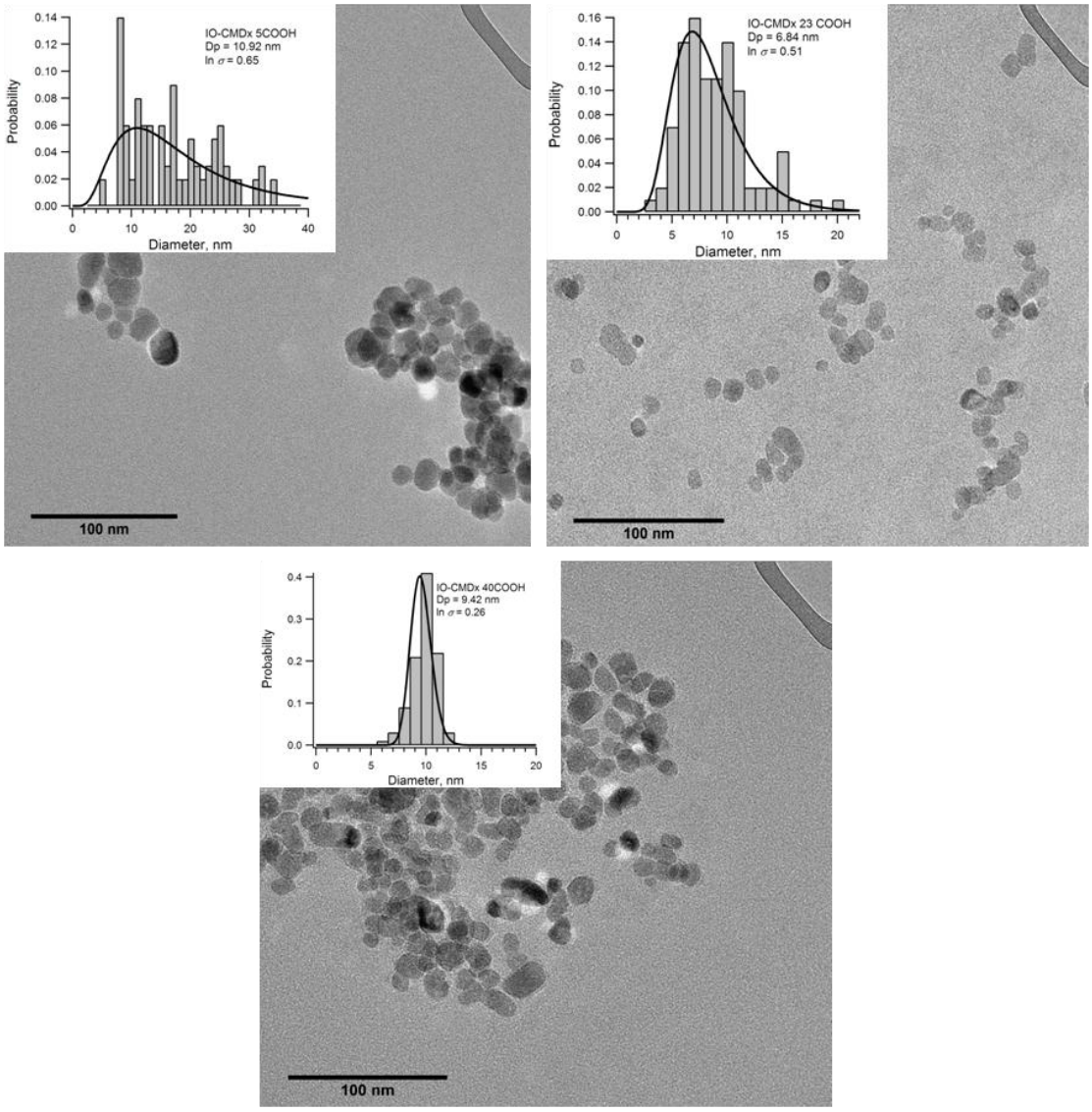

Figure 21. Representative TEM image of iron oxide magnetic nanoparticles synthesized by the co-precipitation method coated with CMDx with different degrees of carboxylic group substitutions.

6.2.2 Dynamic Light Scattering and Zeta Potential measurements

Figure 18 presents a summary of nanoparticle's surface charge as a function of pH. A significant difference between the surface charge at pH ≈ 7.4 between CMDx 23 COOH and CMDx 40 COOH coated nanoparticles was not observed.

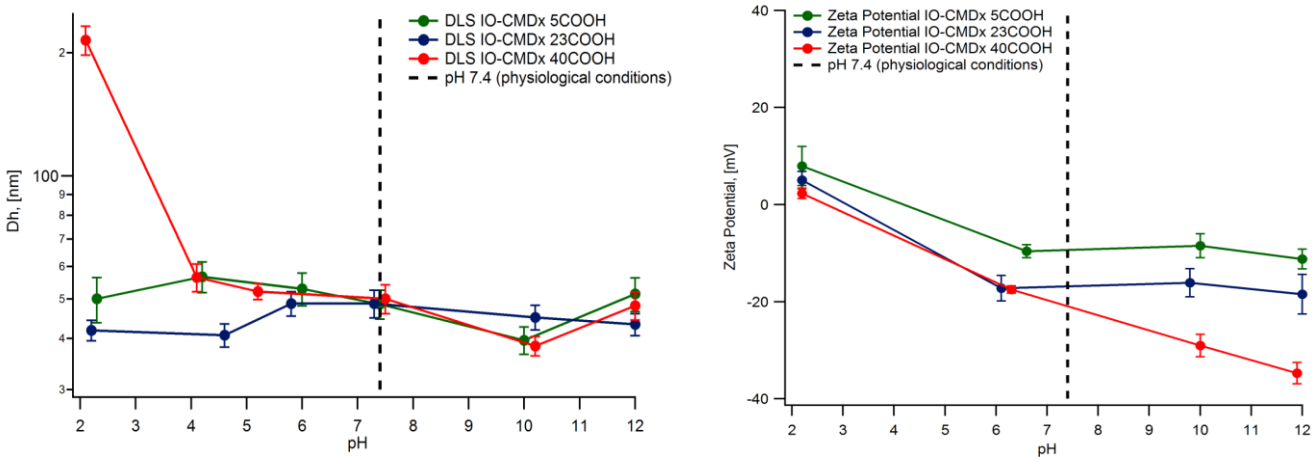

Figure 22. DLS and Zeta potential measurements of CMDx coated nanoparticles with different degrees of substitution.

After 1 week of suspension, no visible aggregates were observed in the bottom of the solutions. This indicates that the CMDx coated magnetic nanoparticles synthesized by co-precipitation method are stable for at least 72 hours. Colloidal stability against pH demonstrated that steric stabilization of magnetic nanoparticles was stronger in contrast to electrostatic stabilization. Systems that are sterically stabilized tend to remain well dispersed even at high salt concentrations or under conditions where the zeta potentials of the surfaces are reduced to near zero, as it was demonstrated before in Ayala's M.S. thesis work.

6.2.3 TGA measurements

The TGA measurements of CMDx coated nanoparticles are provided in Table 4.

Table 4. TGA measurements of CMDx coated nanoparticles

Particles	Average, % of magnetic core	Std Deviation, % of magnetic core
IO-CMDx5COOH	11.68	0.66
IO-CMDx23COOH	16.81	0.93
IO-CMDx40COOH	17.07	0.92

The percent of magnetic core after functionalization with CMDx polymers was determined using TGA measurements. In Table 4, a summary of magnetic core remnants can be observed. The highest value was obtained for IO CMDx 40 nanoparticles with 17% ± 0.92% of magnetic core.

6.2.4 Magnetic properties

In order to understand magnetic properties and estimate core diameter of the CMDx coated nanoparticles, magnetization vs. magnetic field measurements were performed at 300K. The Langevin-Chantrell correlation was used to estimate magnetic core. CMDx 5COOH coated nanoparticles had a magnetic core of 10.27nm ± 0.17 nm with a saturation moment of 63.20 emu/g. CMDx 23 COOH coated nanoparticles had a magnetic core of 9.86nm ± 0.07 nm with a saturation moment of 27.16 emu/g. CMDx 40 COOH coated nanoparticles possess a magnetic core of 9.87nm ± 0.14 nm with a saturation moment of 28.7 emu/g. At 300K, all the samples exhibit super-paramagnetic behavior.

In contrast with CMDx coated nanoparticles, the magnetic core of APS coated nanoparticles was 9.85nm ± 0.04 nm showing a super-paramagnetic behavior with a saturation moment of 73.47 emu/g. On the other hand, peptized magnetic nanoparticles presented a core diameter of about 8.62 nm ± 0.02 nm with a saturation moment of 107.32 emu/g. However, it is known that iron

oxides (e.g., magnetite, maghemite) and ferrites typically have a bulk saturation magnetization of ~90emu/g. For this reason, the value 107.32 emu/g is superior to the values expected.

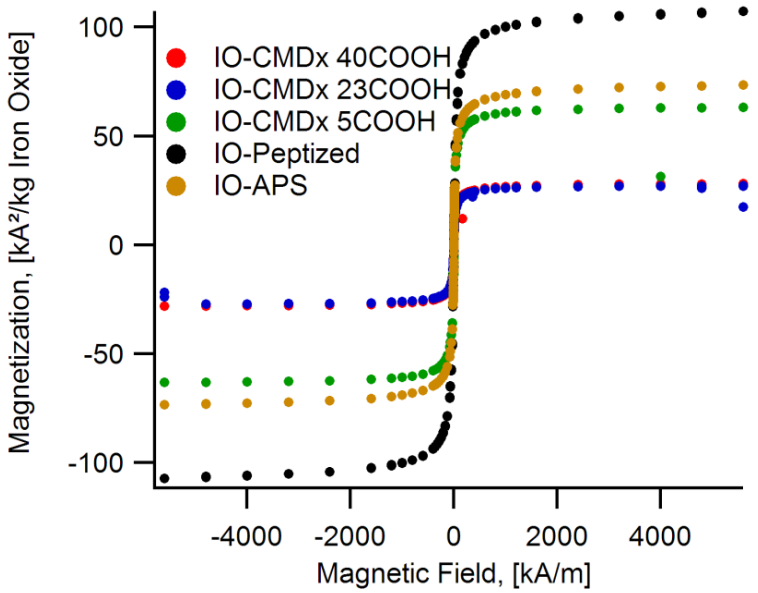

Figure 23. Saturation magnetization at 300K of peptized, APS, CMDx 5COOH, CMDx 23 COOH and CMDx 40 COOH coated nanoparticles.

In this section, successful functionalization of magnetic nanoparticles synthesized via the co-precipitation method with synthesized carboxymethyl-dextran was performed via carbodiimide chemistry. Surface charge of nanoparticles was evaluated by zeta potential measurements as a function of pH. A significant difference was not observed between the surface charge at physiological pH between CMDx 23 COOH- and CMDx 40 COOH- coated nanoparticles. The stability of the particles was studied by measuring the hydrodynamic diameter of magnetic nanoparticles during Dynamic Light Scattering Analyses. No visible aggregation of suspensions was observed.

6.3 Colloidal stability studies in biological buffers

Figures 20 and 21 provides the results of colloidal stability studies obtained at different times and temperatures for PEGSilane2000 and PEGSilane5000 coated nanoparticles. PEGSilane coated nanoparticles did not precipitate at 72 hours of observation. The hydrodynamic diameters changed without a clear tendency as a function of temperature and time. In the range of biological buffers studied, nanoparticle stability was observed.

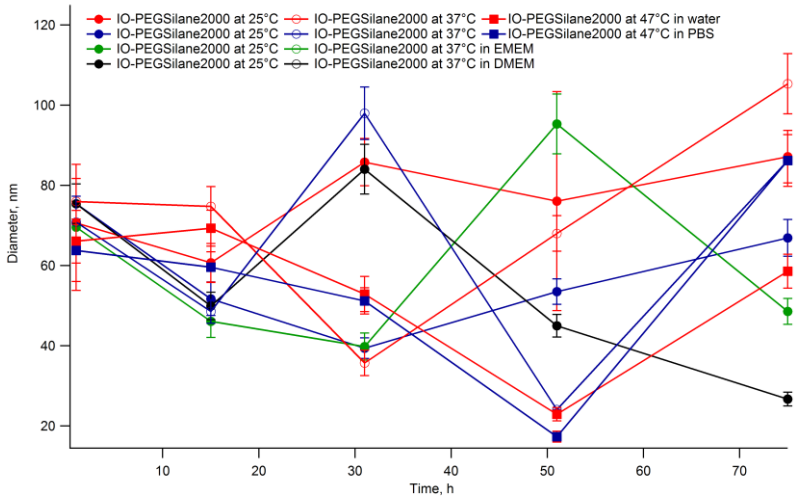

Figure 24. Summary of colloidal stability study of PEG-Silane2000 coated nanoparticles against time and temperature.

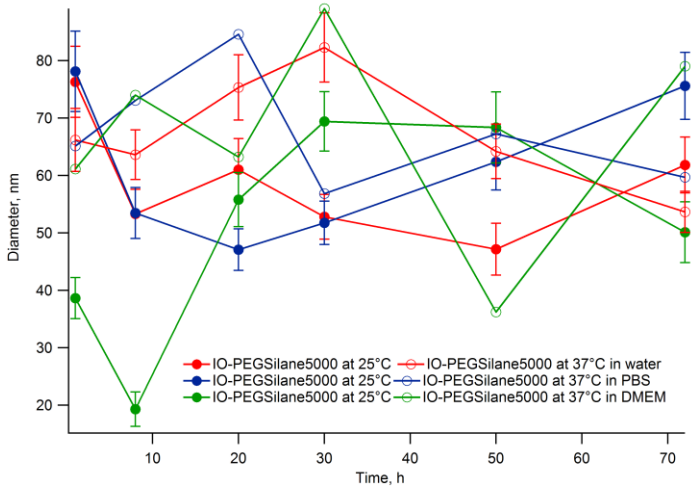

Figure 25. Summary of colloidal stability study of PEG-Silane5000 coated nanoparticles against time and temperature.

Iron oxide nanoparticles coated with PEGSilane polymers showed to be stable in common cell culture media such as DMEM, PBS, and water, even after sterilization by autoclave at 121^{o}C. PEGSilane5000 colloidal stability results in cell culture media were completely different in contrast with DLS and zeta potential measurements in water against pH. Particles appeared colloidally stable despite unsuccessful reproducibility in the preparation of these particles. Primarily, this situation could be due to the fact that particles suspended in cell culture media changes media pH to values lower than 5. Before, it was concluded that at pH lower than 5, particles are electrostatically stable. The question that needs to be asked is where these charges could originate. This could be due to the various components in cell culture media, such as salts, proteins, and glucose.

6.4 Development of a protocol to study protein-nanoparticle interactions by trial and error experiments

A preliminary protocol was prepared to test the capability of Amicon Ultra 4 centrifugal devices to retain particles and remove unbound proteins in nanoparticle-protein interactions studies, using commercial CMDx-coated nanoparticles (detailed procedure is described in appendix D). These studies were done in triplicate as shown in figure 26. Data not shown includes DLS, Zeta potential, and TGA measurements of particles before and after incubation with BSA and LYZ proteins. The adsorption of lysozyme onto the surface of CMDx coated nanoparticles was higher in contrast with the value for BSA. As a result of this previous experimental design, it was theorized that this could be due to differences in surface charge at physiological pH for each protein. Electrostatic interactions between the positive surface charge in LYZ and the negative surface charge of CMDx coated nanoparticles could potentially contribute to protein-nanoparticle interactions (2.20 ± 0.14 mgLYZ/mgcore). BSA possesses a negative surface charge, as do CMDx-coated nanoparticles at pH close to 7. For this reason there are less electrostatic interactions between BSA and CMDx-coated particles (0.60±0.10 mgBSA/mgcore).

Zeta potential measurements for samples showed statistically significant differences with respect to LYZ–nanoparticle complexes and the control nanoparticle solutions. BSA- nanoparticle complexes were not statistically different to nanoparticle control solutions. It was concluded that the electrostatic interactions between positive and negative charges play a pivotal role in protein-nanoparticle interactions. Also, slight changes in the intensity size distribution of particles after treatment with LYZ solution were observed in contrast with the control. After BSA treatment, changes in intensity size distribution of particles were observed. However, this is probably due to the fact that BSA protein, which is a large protein in contrast with LYZ, affected the optical quality of the DLS measurements. TGA measurements did not show the expected results. Commercial CMDx-coated nanoparticles that have not been incubated with protein present a magnetic core around 9.91%. It was expected that the incorporation of proteins onto the magnetic nanoparticle surface would reduce the magnetic core for each sample, especially for

nanoparticles incubated with LYZ, due to the higher percent of protein adsorption. Instead, an increase of magnetic core for particles incubated with LYZ and BSA was observed. In addition, a plateau in the protein-nanoparticles plots was not observed either.

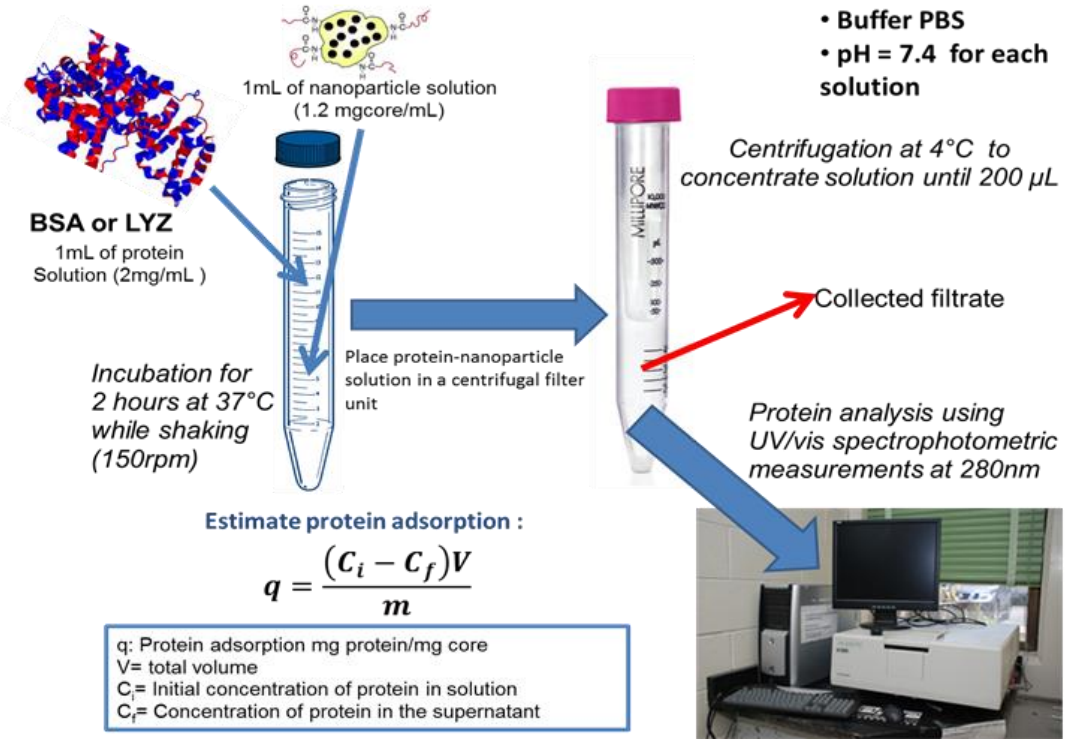

Figure 26. Preliminary protocol used to study BSA and LYZ adsorption onto commercial CMDx-coated nanoparticle surface.

From these results it can be concluded that: i) DLS measurements of nanoparticle-protein complexes are not reliable due the signal of unbound proteins in the system. ii) Zeta potential measurements can give an idea of interaction nature but it is not a reliable technique. It is not clear if signal is due the unbound protein in the system or to strong protein-nanoparticle interactions. iii) TGA measurements do not reflect the decrease in nanoparticle magnetic core that would be expected due to protein-nanoparticle interactions. For these reasons, the use of DLS, Zeta potential, or TGA measurements in future experiments of this nature is not recommended.

6.4.1 Retention experiments

In order to test protein-binding and retention of proteins in Amicon and Pall centrifugal devices, a set of experiments was performed to estimate amount of protein that remained in filter supernatant, membrane and filtrate. Various concentrations of LYZ, BSA and other plasma proteins were centrifuged at 14,000 g for 10min at 4°C (following manufacturer specifications, n = 1). Protein quantification using BCA assay was performed for each filtered solution after each centrifugation and wash step. Mass balance calculations taking into account the amount of filtered protein and initial protein mass were realized in order to estimate bound proteins as percent of retention value in the centrifugal devices. Calibration curves were prepared with BSA standard solution for experiments with BSA and with known solutions of protein for LYZ, TRANS, IgG, and FIBR experiments. Figure 27 and Figure 28 provide an overview of these results.

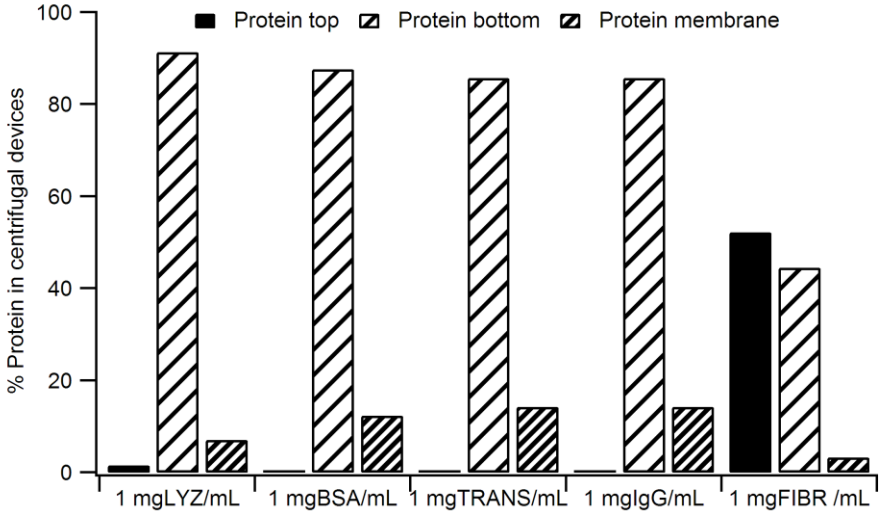

Figure 27. Retention experiments at 14,000g for 10 min at 4°C in Amicon Ultra 100K 0.5 devices (LYZ protein) and Pall Nanosep 300K devices (BSA, TRANS, IgG, FIBR proteins) at low concentrations (n=1).

Protein retention values in centrifugal devices at 14,000g for 10min at 4°C were lower than 20% using LYZ, BSA, TRANS and IgG proteins. These values are not in agreement with the manufacturer specifications (Pall Corporation), because at a concentration of 1mg/mL of BSA and IgG, typical retentate recovery is approximately 2%. Manufacturer did not report at which temperature experiments should be performed. This retention is a function of the protein concentration as shown in Figure 28, due the increase of protein retained in the membrane in LYZ, TRANS and FIBR studies. Retention is also a function of the molecular shape-size of proteins and degree of hydration, counter ions, and steric effects; this can cause molecules with similar molecular weights to exhibit different retention behaviors.

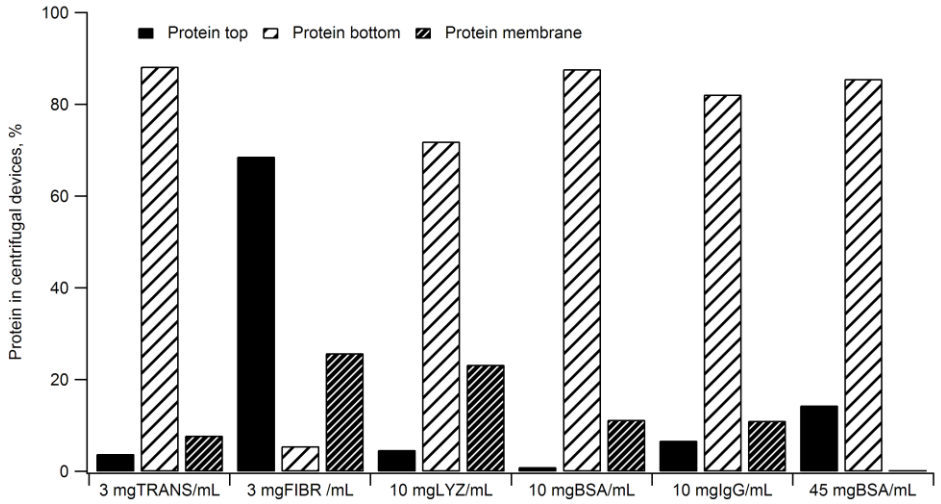

Figure 28. Retention experiments at 14,000g for 10 min at 4°C in Amicon Ultra 100K 0.5 devices (LYZ protein) and Pall Nanosep 300K 0.5 devices (BSA, TRANS, IgG, FIBR proteins) at higher concentrations (n=1).

After several repetitions of these experiments, similar retention values were obtained (data not shown). In this sense, the explanation for these results could be that at high spin velocities, concentration polarization is observed mostly in all studied proteins. Concentration polarization is the accumulation of proteins in a thin layer adjacent to the membrane surface that may interfere with passage of the other proteins through the membrane and can adversely affect the flow rate.

To minimize concentration polarization behavior, low spin rates, long centrifugation times and an increase in temperature where evaluated in a new experiment set using only Amicon Ultra 100K devices. Nanosep devices were not used because they do not completely retain particles in the membrane, as do Amicon devices. Figure 29 shows that BSA retention did not show a considerable change, but in LYZ retention experiments, the percent of protein retention in the membrane is reduced to 8%.

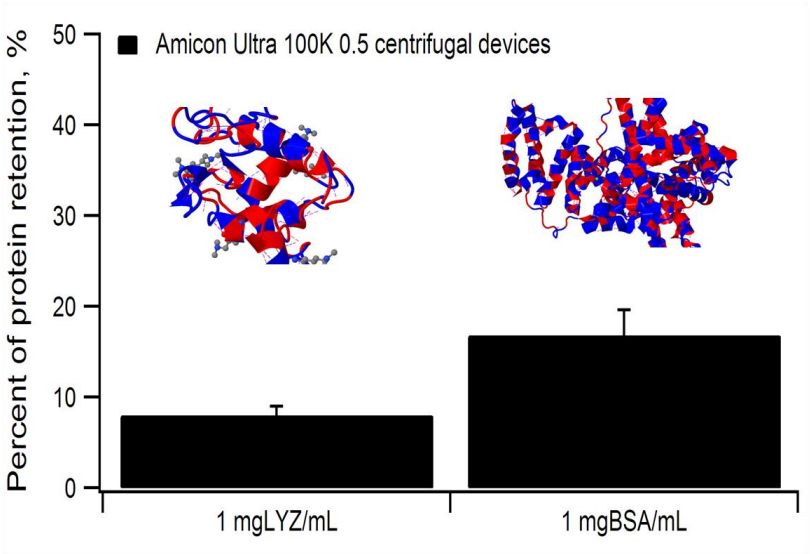

Figure 29. Membrane retention experiments at 1,500g for 20 min at 25°C in Amicon Ultra 100K devices at 1mg of protein per mL (n=4).

Theoretical calculations in order to estimate the protein that can be adsorbed onto the nanoparticles surfaces neglecting electrostatic interactions in experimental conditions were performed and showed in table 4.

Calculations were prepared assuming: (i) 250µL of 1 mgcore/mL particles solutions, (i) 250µL of 2mg/mL BSA and LYZ protein solutions, (iii) hydrodynamic diameter of coated particles in PBS at 37ºC (data presented in table 5). The surface area of the projection of a BSA molecule on the surface in an ultimately filled monolayer is 23 nm^2 in contrast with 10 nm^2 per a single lysozyme molecule in its native state. With the results shown for the conditions selected, it is

possible to quantify protein adsorbed using BCA assay because theoretical protein values are far above from the BCA assay limits of detection.

Table 5. Theorical BSA and LYZ mass per amoung of particle.

Particles	Theoretical BSA mass per amoung of particle, mg	Theoretical LYZ mass per amoung of particle, mg
IO-CMDx 5COOH	1.2137	0.6125
IO-CMDX 23 COOH	0.8433	0.4256
IO-CMDX 40 COOH	1.0649	0.5374
IO-PEGSilane2000	0.3308	0.1669
IO-PEGSilane5000	0.7812	0.3942

6.4.2 Final protocol to study protein-nanoparticle interactions

Finally, studies for proteins-nanoparticles interactions were carried out according to the following protocol after analyzing the results of several preliminary experiments (see figure 30):

a. Prepare stock lysozyme (LYZ) solution adding 12mg of LYZ in 6 mL PBS solution (2mg LYZ/mL concentration).
b. Prepare stock Bovine Serum Albumin (BSA) solution adding 12mg of BSA in 6mL PBS solution (2mg BSA/mL concentration).
c. Prepare stock of CMDx and PEG-Silane coated nanoparticles solutions of 1mgcore/mL concentration (particle core percentages are presented in Table 4).
d. Place 300µL of stock LYZ solution and 300µL particle solution in an eppendorf tube. Quadruple samples.
e. Place 300µL of stock BSA solution and 300µL particles solution in an eppendorf tube. Quadruple samples.
f. Incubate protein-nanoparticle solution at 37°C for 2 hours in a heat block.
g. Centrifuge LYZ-nanoparticle solutions at 1500 g for 20 min at 25°C using Amicon 100K 0.5mL ultracentrifugation devices to obtain 20µL of filtrate.
h. Centrifuge BSA-nanoparticle solutions at 1500 g for 20 min at 25°C using Amicon 100K 0.5mL ultracentrifugation devices to obtain 20µL of filtrate.

i. Recover filtrate in order to quantify proteins in solution using BCA assay.

j. Rinse ultracentrifugation device three times with PBS in order to remove free protein in solution.

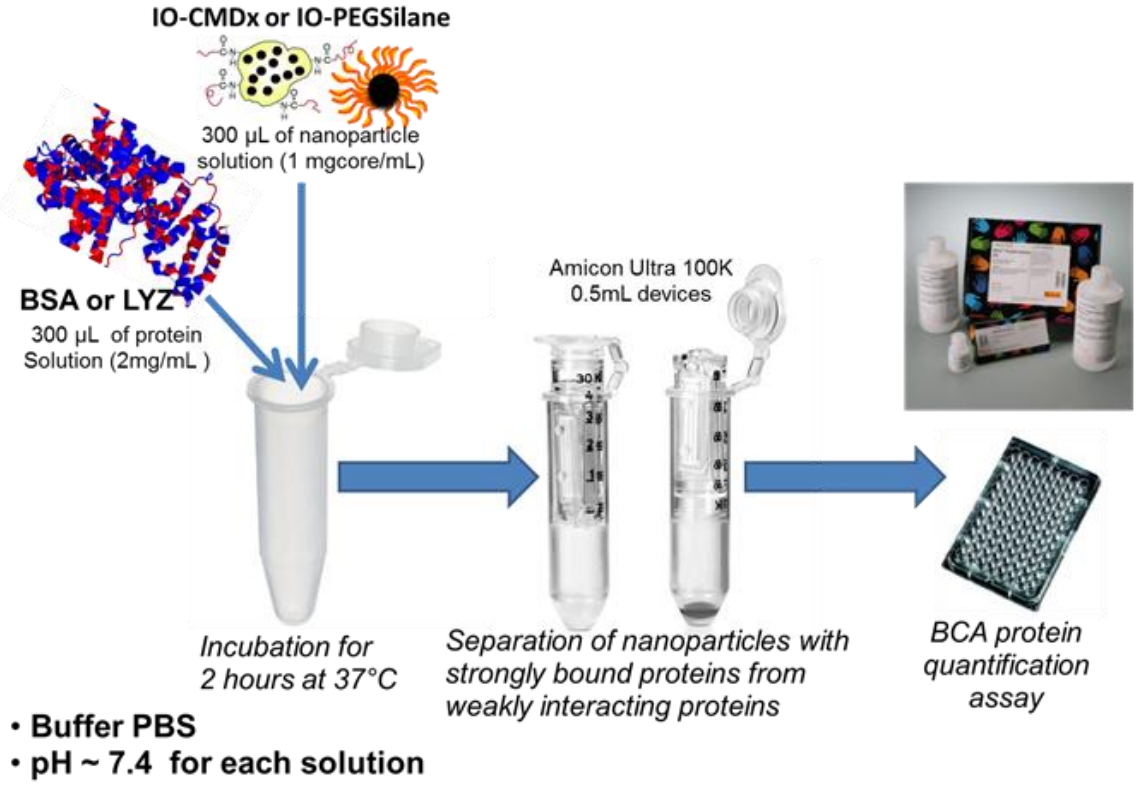

Figure 30. Final protocol to quantify protein-nanoparticle interactions using Amicon Ultra 100K 0.5mL devices and BCA assay.

Detail of magnetic nanoparticles suspended in PBS for experiments are presented in table 6:

Table 6. TEM, DLS and TGA measurements of CMDx and PEGSilane coated nanoparticles.

Particles	Dcore TEM,	Dh, nm At 37ºC, PBS $1mg_{particles}/mL$	TGA, % magnetic core
IO-CMDx 5COOH	10.92 nm lnσ= 0.65	51.20 ± 3.32	11.68 ± 0.66
IO-CMDX 23 COOH	6.84 nm lnσ= 0.51	51.20 ± 3.32	16.81 ± 0.93
IO-CMDX 40 COOH	9.42 nm lnσ= 0.26	39.93 ± 2.43	17.07 ± 0.92
IO-PEGSilane2000	8.94 nm lnσ= 0.41	60.78 ± 4.18	36.10 ± 1.62
IO-PEGSilane5000	7.21 nm lnσ= 0.39	72.76 ± 6.12	12.77 ± 1.79

In general, retention of proteins in the membrane of Amicon Devices was observed. In order to estimate protein retention for the conditions described above, retention experiments were performed at 1mg/mL of protein as described previously. Results showed 16.82% ± 2.75% retention for BSA and 8.04% ± 0.94% for LYZ. Particles go through the Amicon membrane at the conditions tested. BCA assay was used to calculate signal contribution of nanoparticles (without protein), since BCA assay detects peptide bond in proteins. Filtrate after each centrifugation and wash step was analyzed using BCA assay. This experiment showed that particles go through the membrane in the 1st centrifugation and that there is no evidence of particle signal in the filtrate of the following wash steps. This signal was taken into consideration as a background signal for mass balance calculations.

Although experimental conditions for all samples were the same, the filtrate volume for each sample is not constant. For these experiments, it was assumed that typical final supernatant volume is 20μL, which means the final filtrate volume is 480 μL. The assumption that the first centrifugation removes weakly interacting or unbound proteins from strong protein-nanoparticle complexes using BCA assay is not clear, and CFDs presented certain retention level. Also, to assume that three wash steps with PBS to remove weakly bound proteins from nanoparticles into the filtrate is not clear using this experimental design.

Here were determined that employing a denaturation process with detergent (Sodium Duodecyl Sulfate, or SDS) and temperature *after* centrifugation and wash steps was not appropriate because concentration of proteins in the filtrate as determined by BCA assay was below the detection limit. The most reasonable way to estimate protein adsorption onto nanoparticle surface is by taking into consideration the amount of protein retained on the ultracentrifugation device membrane, initial protein mass, and protein concentration in the filtrate, via calculations using mass balance. However, by taking the retention mass per sample into consideration, negative results were obtained in some cases.

6.5 Protein-nanoparticle interactions results

The protocol developed for protein-nanoparticle interactions study has strong limitations in terms of obtaining accurate values of protein adsorption at the specified operating conditions selected for this analysis. However, the possibility of fine-tuning this protocol for use in further experiments should not be excluded after optimization of certain parameters, such as: protein concentration, spin velocity, time, and temperature, depending on protein-nanoparticle complexes. Results suggest protein-nanoparticle interactions are too weak to be measured completely by the protocol described in these studies.

Nevertheless, it was observed that for LYZ, the percent of retention remains constant throughout the experiments (see Figure 31). However, protein quantification after wash steps to remove unbound proteins at the nanoparticles surface was affected considerably because of volume errors. This error is due to the fact that for membrane retention calculations, it was assumed that the ultracentrifugation devices have a typical supernatant volume of 20uL, equivalent to 0.48mL of filtrate after each centrifugation. Another observation is that without the wash steps, there is clearly a membrane retention problem that is higher in BSA than LYZ studies at 1mg protein/mL. This difference is primarily due to the differences in molecular weight of each protein.

With these findings, it has been demonstrated that the conditions under which centrifugations and subsequent washes are done are critical for interaction studies. Additionally, quantification of protein-nanoparticle interactions is a complicated issue, which cannot be accurately estimated with the current protocol. Figure 31 shows the final results after centrifugation and rinse protocols using CFDs. For final protein-adsorption calculations retention, results were obtained using as final values the protein adsorbed the after the third wash.

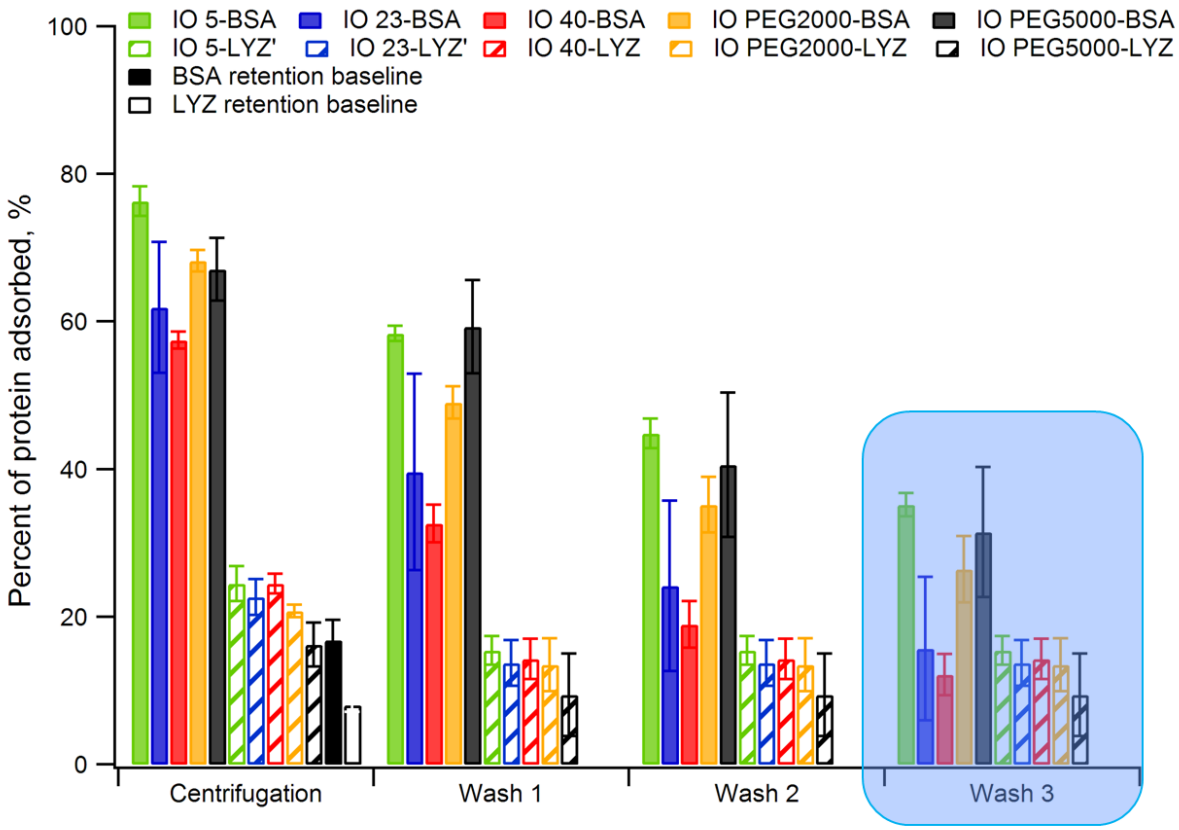

Figure 31. Retention tendencies for protein-nanoparticle complexes after centrifugation and rinse steps in Amicon Ultra 100K 0.5 centrifugal devices (n=4).

In figure 32 there appear to be clear differences between BSA and LYZ interaction behavior with nanoparticle with different surface characteristics. IO 5 nanoparticles, PEG2000-, and PEG5000- coated nanoparticles interacted with BSA proteins presumably due to the presence of unreacted amine groups. Since carboxylic groups are bigger than amine groups, IO 23 and IO 40 nanoparticles interact in a repulsive way with BSA proteins (like charges repel like). In this case, the results suggest that there are no interactions between nanoparticles and BSA protein, because calculated levels of protein interacting with nanoparticles were lower than levels of Amicon 100K membrane retention.

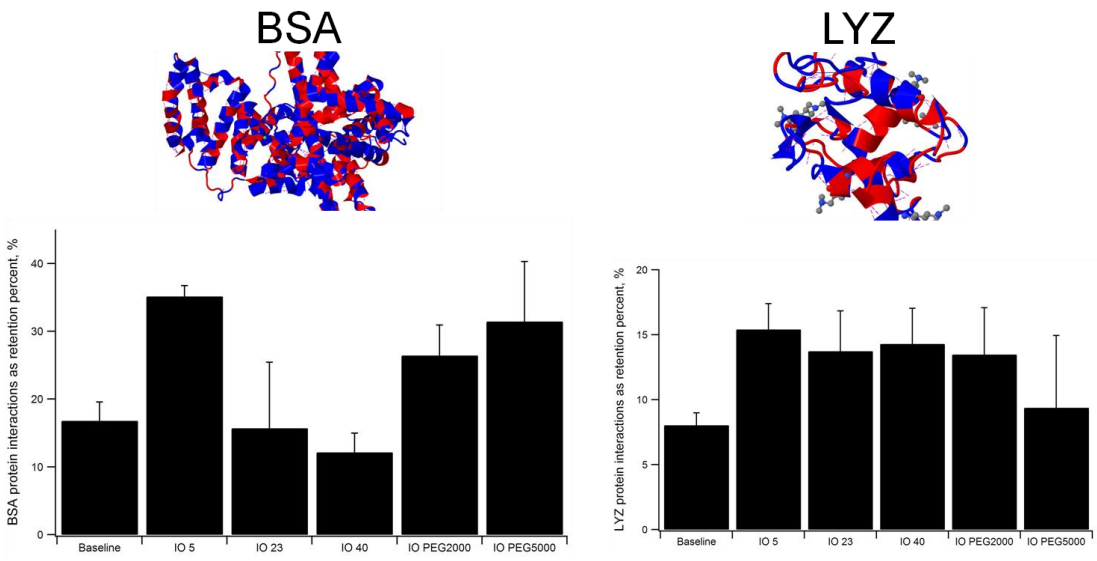

Figure 32. Protein-nanoparticle interactions in presence of BSA and LYZ proteins at 1mg/mL after 2 hours of incubation time at 37ºC (n=4).

In the case of LYZ, there seems to between similar levels of interaction between IO 5, IO 23, IO 40 and IO PEGSilane2000 nanoparticles. LYZ interactions with IO PEGSilane5000 seem lower, but it is not a statistically significant difference. This is probably due to polarization concentration and membrane fouling effects.

For future experiments it is recommended that aditional proteins or molecules in order to mimic bloodstream and biological fluid conditions be used. We highly recommend the use of histones (HIS) and trypsin (TRY) proteins (14 kDa and 23.3 kDa, respectively) as models to study nanoparticle interactions with positive proteins at physiological pH. The use of Fetal Bovine Serum (FBS), hemoglobin from bovine blood (64.5 kDa), and myoglobin from equine skeletal muscle as models to study interactions with negative proteins at physiological pH is also recommended. Interactions with glucose, whole blood, blood serum and plasma should be studied due to the high presence of glucose in the blood stream to attempt to mimic *in vivo* conditions in complex biological systems using blood components as a whole. The method employed for quantitating proteins in solution will depend on the measurement range.

Absorbance at 280nm or BCA assay can be used for BSA and LYZ proteins (50µg/mL to 2mg/mL measurement range). The protocol described above was effective for recognizing problems and identifying possible solutions to more accurately develop a system that can effectively determine interactions between various proteins and nanoparticles with different surface characteristics.

Finally, a protocol intended to study interactions between proteins and magnetic nanoparticles with various surface characteristics was developed with several limitations, such as membrane fouling, polarization concentration, and protein retention in CFDs.

6.6 Protein and particle sedimentation studies

For 1 and 10 mg of protein per mL, sedimentation or precipitation of proteins was not observable using BCA assay. Protein sedimentation at 60 mg of protein per mL was appreciable using BCA assay. Figure 33 shows details of these results:

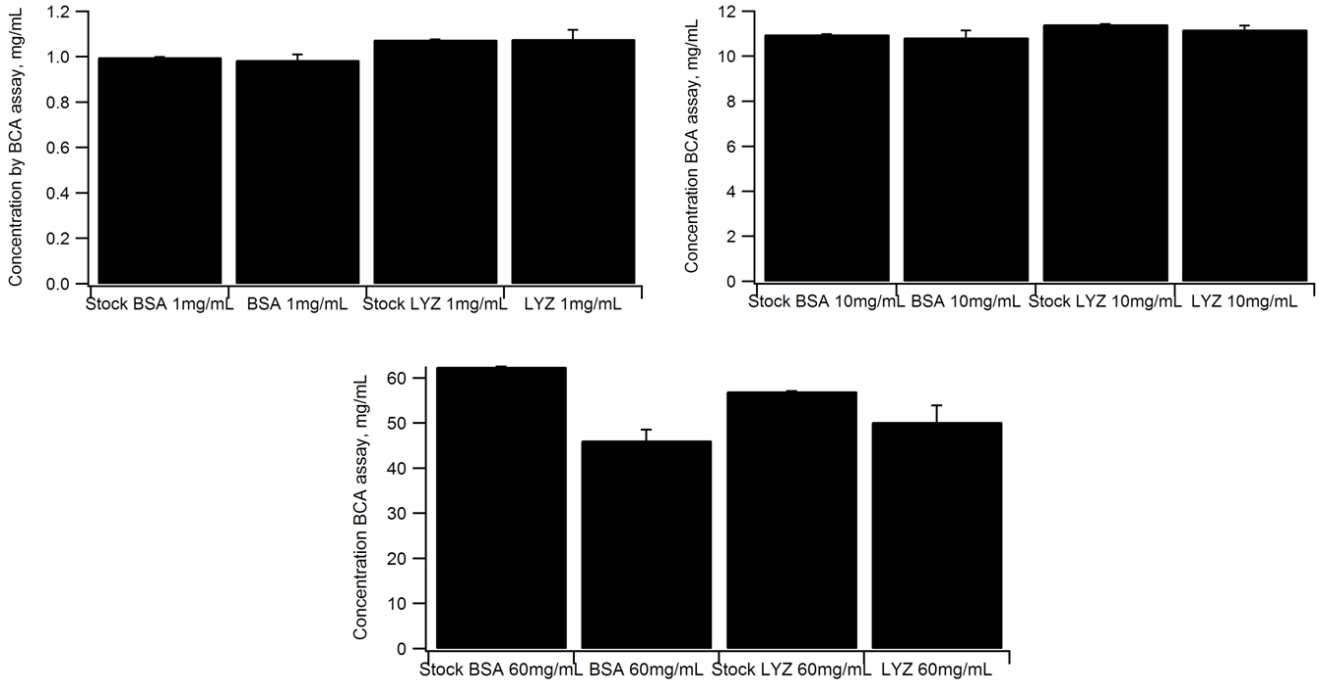

Figure 33. BSA and LYZ protein sedimentation at ~21,000g for 80min at 4°C

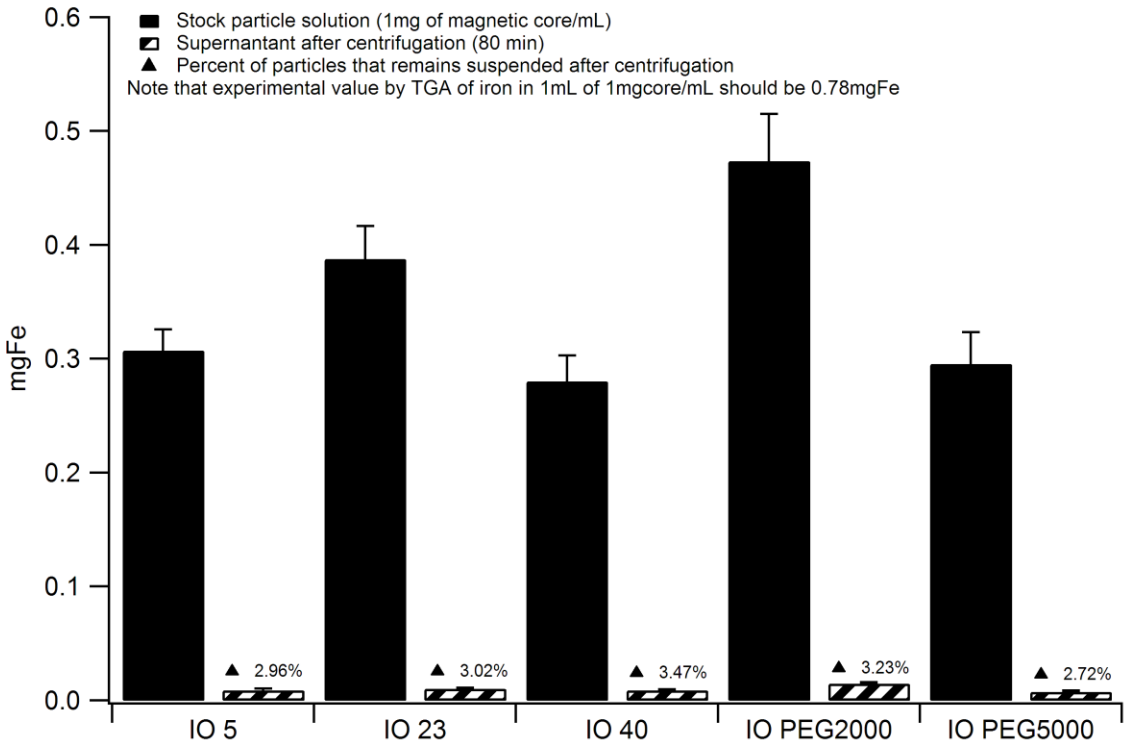

Figure 34. Iron content (Fe) in particle stock solution and centrifugation supernatants.

Iron is an interfering substance in the BCA assay. Experiments with centrifugal filter devices showed that particles have signal in the UV/Vis readings. Fe concentration by UV/Vis measurements is lower than the TGA experimental value for 1mL of 1mg of core per mL solution (assuming magnetite magnetic core). Stock solutions are not homogeneous samples. For this reason a concentration of 1 mg of core per mL has different iron content for each type of particle.

7 CONCLUSIONS AND FUTURE WORK

7.1 Conclusions

An easy and effective method was developed for chemical coating of magnetic nanoparticles synthesized by the coprecipitation method with PEG-Silane polymers of different molecular weights. PEGSilane2000 coated nanoparticles were stable against all pH conditions tested at room temperature. In the range of biological buffers studied, stability was observed for PEGSilane5000 coated nanoparticles.

Ultracentrifugation using Centrifugal Filter Devices is not recommended as a tool to study protein-nanoparticle interactions, because of protein retention in filter membranes due to membrane fouling and concentration polarization at the experimental conditions tested. However, to have an idea of the nature of protein-nanoparticle interactions CFDs could be carefully selected for each protein-particle complex, taking into account critical variables such as g-force, centrifugation time, protein concentration and temperature.

7.2 Future work

Future work should include *in situ* monitoring of the nanoparticle protein corona with the above cited proteins using more precise methods, such as optical birefringence signal induced by an external magnetic field or AC susceptibility measurements with thermally blocked magnetic nanoparticles in order to obtain a real idea of the behavior of protein-nanoparticle interactions. These studies must include protein interactions against nanoparticle concentration, macromolecular crowding of proteins, and the effect of ionic strength in protein-nanoparticle solutions.

8 REFERENCES

[1] A. Figuerola, R. Di Corato, L. Manna, and T. Pellegrino, "From iron oxide nanoparticles towards advanced iron-based inorganic materials designed for biomedical applications," *Pharmacological Research*, vol. 62, no. 2, pp. 126–143, Aug. 2010.

[2] A. K. Gupta and M. Gupta, "Synthesis and surface engineering of iron oxide nanoparticles for biomedical applications," *Biomaterials*, vol. 26, no. 18, pp. 3995–4021, Jun. 2005.

[3] A. Tomitaka, T. Koshi, S. Hatsugai, T. Yamada, and Y. Takemura, "Magnetic characterization of surface-coated magnetic nanoparticles for biomedical application," *Journal of Magnetism and Magnetic Materials*, vol. 323, no. 10, pp. 1398–1403, May 2011.

[4] S.-D. Li and L. Huang, "Pharmacokinetics and Biodistribution of Nanoparticles," *Mol. Pharmaceutics*, vol. 5, no. 4, pp. 496–504, 2008.

[5] S. Park and K. Hamad-Schifferli, "Nanoscale interfaces to biology," *Current Opinion in Chemical Biology*, vol. 14, no. 5, pp. 616–622, Oct. 2010.

[6] S. F. Medeiros, A. M. Santos, H. Fessi, and A. Elaissari, "Stimuli-responsive magnetic particles for biomedical applications," *International Journal of Pharmaceutics*, vol. 403, no. 1–2, pp. 139–161, Jan. 2011.

[7] P. Aggarwal, J. B. Hall, C. B. McLeland, M. A. Dobrovolskaia, and S. E. McNeil, "Nanoparticle interaction with plasma proteins as it relates to particle biodistribution, biocompatibility and therapeutic efficacy," *Advanced Drug Delivery Reviews*, vol. 61, no. 6, pp. 428–437, Jun. 2009.

[8] P. P. Karmali and D. Simberg, "Interactions of nanoparticles with plasma proteins: implication on clearance and toxicity of drug delivery systems," *Expert Opin. Drug Deliv.*, vol. 8, no. 3, pp. 343–357, 2011.

[9] F. Meder, T. Daberkow, L. Treccani, M. Wilhelm, M. Schowalter, A. Rosenauer, L. Mädler, and K. Rezwan, "Protein adsorption on colloidal alumina particles functionalized with amino, carboxyl, sulfonate and phosphate groups," *Acta Biomaterialia*, vol. 8, no. 3, pp. 1221–1229, Mar. 2012.

[10] S. Karimi, T. Nickchi, and A. Alfantazi, "Effects of bovine serum albumin on the corrosion behaviour of AISI 316L, Co–28Cr–6Mo, and Ti–6Al–4V alloys in phosphate buffered saline solutions," *Corrosion Science*, vol. 53, no. 10, pp. 3262–3272, Oct. 2011.

[11] M. Creixell, A. P. Herrera, M. Latorre-Esteves, V. Ayala, M. Torres-Lugo, and C. Rinaldi, "The effect of grafting method on the colloidal stability and in vitro cytotoxicity of carboxymethyl dextran coated magnetic nanoparticles," *J. Mater. Chem.*, vol. 20, no. 39, pp. 8539–8547, 2010.

[12] "Biomed Imaging Interv J 2010; 6(2):e12 - Development and use of iron oxide nanoparticles (Part 1): Synthesis of iron oxide nanoparticles for MRI." [Online]. Available: http://www.biij.org/2010/2/e12/. [Accessed: 20-Nov-2011].

[13] R. Massart, "Preparation of aqueous magnetic liquids in alkaline and acidic media," *Magnetics, IEEE Transactions on DOI - 10.1109/TMAG.1981.1061188*, vol. 17, no. 2, pp. 1247–1248, 1981.

[14] J. Park, K. An, Y. Hwang, J.-G. Park, H.-J. Noh, J.-Y. Kim, J.-H. Park, N.-M. Hwang, and T. Hyeon, "Ultra-large-scale syntheses of monodisperse nanocrystals," *Nat Mater*, vol. 3, no. 12, pp. 891–895, Dec. 2004.

[15] S. G. Kwon and T. Hyeon, "Formation Mechanisms of Uniform Nanocrystals via Hot-Injection and Heat-Up Methods," *Small*, vol. 7, no. 19, pp. 2685–2702, 2011.

[16] S. Jo and K. Park, "Surface modification using silanated poly(ethylene glycol)s," *Biomaterials*, vol. 21, no. 6, pp. 605–616, Mar. 2000.

[17] C. Barrera, A. P. Herrera, and C. Rinaldi, "Colloidal dispersions of monodisperse magnetite nanoparticles modified with poly(ethylene glycol)," *Journal of Colloid and Interface Science*, vol. 329, no. 1, pp. 107–113, Jan. 2009.

[18] E. K. U. Larsen, T. Nielsen, T. Wittenborn, H. Birkedal, T. Vorup-Jensen, M. H. Jakobsen, L. Østergaard, M. R. Horsman, F. Besenbacher, K. A. Howard, and J. Kjems, "Size-Dependent Accumulation of PEGylated Silane-Coated Magnetic Iron Oxide Nanoparticles in Murine Tumors," *ACS Nano*, vol. 3, no. 7, pp. 1947–1951, 2009.

[19] "ScienceDirect - Bioconjugate Techniques (Second Edition) Home Page." [Online]. Available: http://library.uprm.edu:2051/science/book/9780123705013. [Accessed: 20-Nov-2011].

[20] R. Huynh, F. Chaubet, and J. Jozefonvicz, "Carboxymethylation of dextran in aqueous alcohol as the first step of the preparation of derivatized dextrans," *Angew. Makromol. Chem.*, vol. 254, no. 1, pp. 61–65, 1998.

[21] R. De Palma, S. Peeters, M. J. Van Bael, H. Van den Rul, K. Bonroy, W. Laureyn, J. Mullens, G. Borghs, and G. Maes, "Silane Ligand Exchange to Make Hydrophobic Superparamagnetic Nanoparticles Water-Dispersible," *Chem. Mater.*, vol. 19, no. 7, pp. 1821–1831, 2007.

[22] A. P. Herrera, C. Barrera, and C. Rinaldi, “Synthesis and functionalization of magnetite nanoparticles with aminopropylsilane and carboxymethyldextran,” *J. Mater. Chem.*, vol. 18, no. 31, pp. 3650–3654, 2008.

[23] D. E. Owens III and N. A. Peppas, “Opsonization, biodistribution, and pharmacokinetics of polymeric nanoparticles,” *International Journal of Pharmaceutics*, vol. 307, no. 1, pp. 93–102, Jan. 2006.

[24] M. Egon, “Principles of colloid and surface chemistry: By Paul C. Hiemenz, Marcel Dekker, New York, 1977. 516 pp. $19.50,” *Journal of Colloid and Interface Science*, vol. 70, no. 2, p. 399, Jun. 1979.

[25] Y. Liang, N. Hilal, P. Langston, and V. Starov, “Interaction forces between colloidal particles in liquid: Theory and experiment,” *Advances in Colloid and Interface Science*, vol. 134–135, no. 0, pp. 151–166, Oct. 2007.

[26] A. Petri-Fink, B. Steitz, A. Finka, J. Salaklang, and H. Hofmann, “Effect of cell media on polymer coated superparamagnetic iron oxide nanoparticles (SPIONs): Colloidal stability, cytotoxicity, and cellular uptake studies,” *European Journal of Pharmaceutics and Biopharmaceutics*, vol. 68, no. 1, pp. 129–137, Jan. 2008.

[27] E. Casals, T. Pfaller, A. Duschl, G. J. Oostingh, and V. Puntes, “Time Evolution of the Nanoparticle Protein Corona,” *ACS Nano*, vol. 4, no. 7, pp. 3623–3632, 2010.

[28] M. Jansch, P. Stumpf, C. Graf, E. Rühl, and R. H. Müller, “Adsorption kinetics of plasma proteins on ultrasmall superparamagnetic iron oxide (USPIO) nanoparticles,” *International Journal of Pharmaceutics*, no. 0.

[29] P. Turbill, T. Beugeling, and A. A. Poot, “Proteins involved in the Vroman effect during exposure of human blood plasma to glass and polyethylene,” *Biomaterials*, vol. 17, no. 13, pp. 1279–1287, Jul. 1996.

[30] M. A. Dobrovolskaia, A. K. Patri, J. Zheng, J. D. Clogston, N. Ayub, P. Aggarwal, B. W. Neun, J. B. Hall, and S. E. McNeil, “Interaction of colloidal gold nanoparticles with human blood: effects on particle size and analysis of plasma protein binding profiles,” *Nanomedicine: Nanotechnology, Biology and Medicine*, vol. 5, no. 2, pp. 106–117, Jun. 2009.

[31] J. Christodoulou, P. J. Sadler, and A. Tucker, “1H NMR of albumin in human blood plasma: drug binding and redox reactions at Cys34,” *FEBS Letters*, vol. 376, no. 1–2, pp. 1–5, Nov. 1995.

[32] K. Felix, “Albumin as a drug carrier: Design of prodrugs, drug conjugates and nanoparticles,” *Journal of Controlled Release*, vol. 132, no. 3, pp. 171–183, Dec. 2008.

[33] M. E. Brandsma, A. M. Jevnikar, and S. Ma, “Recombinant human transferrin: Beyond iron binding and transport,” *Biotechnology Advances*, vol. 29, no. 2, pp. 230–238, Apr. 2011.

[34] H. W. Schroeder Jr. and L. Cavacini, “Structure and function of immunoglobulins,” *Journal of Allergy and Clinical Immunology*, vol. 125, no. 2, Supplement 2, pp. S41–S52, Feb. 2010.

[35] C. Fuss, J. C. Palmaz, and E. A. Sprague, “Fibrinogen: Structure, Function, and Surface Interactions,” *Journal of Vascular and Interventional Radiology*, vol. 12, no. 6, pp. 677–682, Jun. 2001.

[36] J. Hankiewicz and E. Swierczek, “Lysozyme in human body fluids,” *Clinica Chimica Acta*, vol. 57, no. 3, pp. 205–209, Dec. 1974.

[37] R. Dommett, M. Zilbauer, J. T. George, and M. Bajaj-Elliott, “Innate immune defence in the human gastrointestinal tract,” *Molecular Immunology*, vol. 42, no. 8, pp. 903–912, May 2005.

[38] P. Kokoshis, D. Williams, J. Cook, and N. Di Luzio, “Increased resistance to Staphylococcus aureus infection and enhancement in serum lysozyme activity by glucan,” *Science*, vol. 199, no. 4335, pp. 1340 –1342, Mar. 1978.

[39] V. Erwin A., “Protein adsorption in three dimensions,” *Biomaterials*, vol. 33, no. 5, pp. 1201–1237, Feb. 2012.

[40] S. H. D. P. Lacerda, J. J. Park, C. Meuse, D. Pristinski, M. L. Becker, A. Karim, and J. F. Douglas, “Interaction of Gold Nanoparticles with Common Human Blood Proteins,” *ACS Nano*, vol. 4, no. 1, pp. 365–379, 2009.

[41] K. Xiao, Y. Li, J. Luo, J. S. Lee, W. Xiao, A. M. Gonik, R. G. Agarwal, and K. S. Lam, “The effect of surface charge on in vivo biodistribution of PEG-oligocholic acid based micellar nanoparticles,” *Biomaterials*, vol. 32, no. 13, pp. 3435–3446, May 2011.

[42] F. Alexis, E. Pridgen, L. K. Molnar, and O. C. Farokhzad, “Factors Affecting the Clearance and Biodistribution of Polymeric Nanoparticles,” *Mol. Pharmaceutics*, vol. 5, no. 4, pp. 505–515, 2008.

[43] S. Rana, Y.-C. Yeh, and V. M. Rotello, “Engineering the nanoparticle–protein interface: applications and possibilities,” *Current Opinion in Chemical Biology*, vol. 14, no. 6, pp. 828–834, Dec. 2010.

[44] D. Phlip, “Supramolecular chemistry: Concepts and perspectives. By J.-M. Lehn, VCH, Weinheim 1995, x, 271 pp., softcover, DM 58.00, ISBN 3-527-2931 1-6,” *Adv. Mater.*, vol. 8, no. 10, pp. 866–868, 1996.

[45] A. J. Cole, A. E. David, J. Wang, C. J. Galbán, H. L. Hill, and V. C. Yang, “Polyethylene glycol modified, cross-linked starch-coated iron oxide nanoparticles for enhanced magnetic tumor targeting,” *Biomaterials*, vol. 32, no. 8, pp. 2183–2193, Mar. 2011.

[46] A. Lesniak, A. Campbell, M. P. Monopoli, I. Lynch, A. Salvati, and K. A. Dawson, “Serum heat inactivation affects protein corona composition and nanoparticle uptake,” *Biomaterials*, vol. 31, no. 36, pp. 9511–9518, Dec. 2010.

[47] A. Bajaj, B. Samanta, H. Yan, D. J. Jerry, and V. M. Rotello, “Stability, toxicity and differential cellular uptake of protein passivated-Fe3O4 nanoparticles,” *J. Mater. Chem.*, vol. 19, no. 35, pp. 6328–6331, 2009.

[48] F. Alexis, E. Pridgen, L. K. Molnar, and O. C. Farokhzad, “Factors Affecting the Clearance and Biodistribution of Polymeric Nanoparticles,” *Mol. Pharmaceutics*, vol. 5, no. 4, pp. 505–515, 2008.

[49] G. Baier, C. Costa, A. Zeller, D. Baumann, C. Sayer, P. H. H. Araujo, V. Mailänder, A. Musyanovych, and K. Landfester, “BSA Adsorption on Differently Charged Polystyrene Nanoparticles using Isothermal Titration Calorimetry and the Influence on Cellular Uptake,” *Macromol. Biosci.*, vol. 11, no. 5, pp. 628–638, 2011.

[50] S. Qin, L. Wang, X. Zhang, and G. Su, “Grafting poly(ethylene glycol) monomethacrylate onto Fe3O4 nanoparticles to resist nonspecific protein adsorption,” *Applied Surface Science*, vol. 257, no. 3, pp. 731–735, Nov. 2010.

[51] L. Lartigue, C. Wilhelm, J. Servais, C. Factor, A. Dencausse, J.-C. Bacri, N. Luciani, and F. Gazeau, “Nanomagnetic Sensing of Blood Plasma Protein Interactions with Iron Oxide Nanoparticles: Impact on Macrophage Uptake,” *ACS Nano*, vol. 6, no. 3, pp. 2665–2678, 2012.

[52] M. Mahmoudi, I. Lynch, M. R. Ejtehadi, M. P. Monopoli, F. B. Bombelli, and S. Laurent, “Protein−Nanoparticle Interactions: Opportunities and Challenges,” *Chem. Rev.*, vol. 111, no. 9, pp. 5610–5637, 2011.

[53] “Determination of plasma protein adsorption on magn... [Pharm Res. 1997] - PubMed - NCBI.” [Online]. Available: http://www.ncbi.nlm.nih.gov/pubmed/9244148. [Accessed: 08-Apr-2012].

[54] B. S. Lele and M. G. Kulkarni, “Single step room temperature oxidation of poly(ethylene glycol) to poly(oxyethylene)-dicarboxylic acid,” *J. Appl. Polym. Sci.*, vol. 70, no. 5, pp. 883–890, 1998.

[55] A. Lopez-Cruz, C. Barrera, V. L. Calero-DdelC, and C. Rinaldi, “Water dispersible iron oxide nanoparticles coated with covalently linked chitosan,” *J. Mater. Chem.*, vol. 19, no. 37, pp. 6870–6876, 2009.

[56] R. Chantrell, J. Popplewell, and S. Charles, “Measurements of particle size distribution parameters in ferrofluids,” *Magnetics, IEEE Transactions on DOI - 10.1109/TMAG.1978.1059918*, vol. 14, no. 5, pp. 975–977, 1978.

[57] R. R.E., “Heating magnetic fluid with alternating magnetic field,” *Journal of Magnetism and Magnetic Materials*, vol. 252, no. 0, pp. 370–374, Nov. 2002.

[58] “ProQuest Document View - Carboxymethylation of dextran for surface modification of magnetite nanoparticles.” [Online]. Available: http://gradworks.umi.com/14/68/1468641.html. [Accessed: 23-Nov-2011].

[59] C. Barrera, A. Herrera, Y. Zayas, and C. Rinaldi, “Surface modification of magnetite nanoparticles for biomedical applications,” *Journal of Magnetism and Magnetic Materials*, vol. 321, no. 10, pp. 1397–1399, May 2009.

[60] “Magnetic iron oxide nanoparticles: synthesis and surface functionalization strategies. | Mendeley”.

9 APPENDIXES

APPENDIX A. X-Ray Measurements

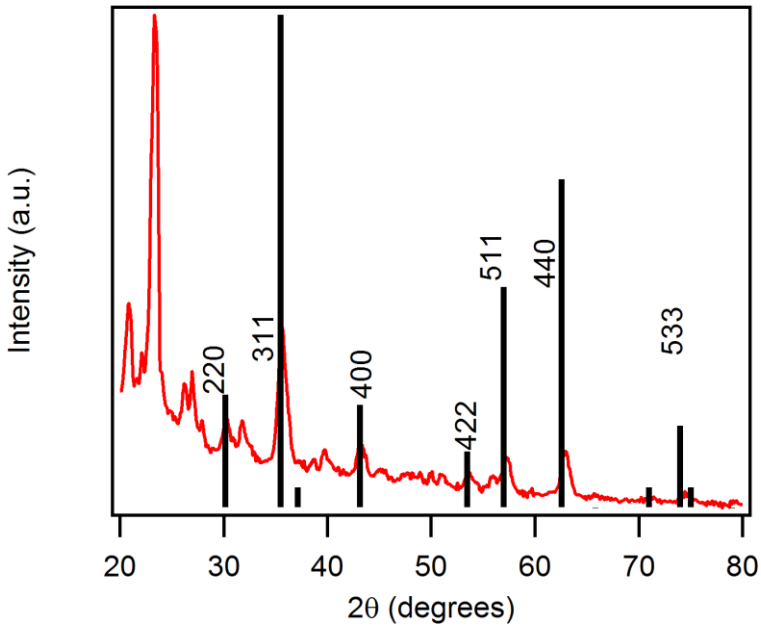

A1.X-ray power diffraction patterns of PEG-Silane5000 coated nanoparticles.

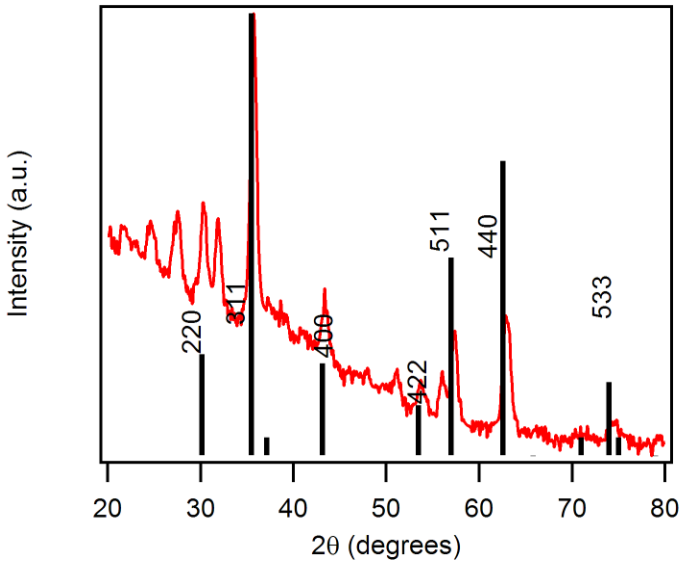

A2.X-ray powder diffraction patterns of CMDx 5COOH coated nanoparticles.

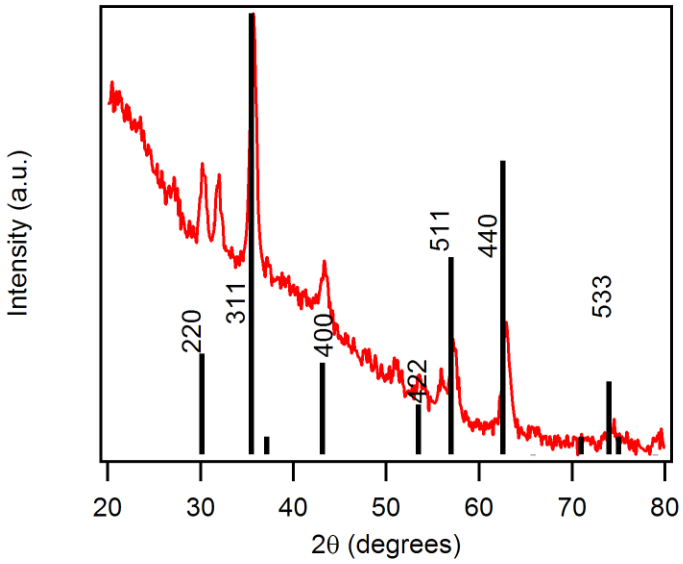

A3.X-ray powder diffraction patterns of CMDx 23COOH coated nanoparticles.

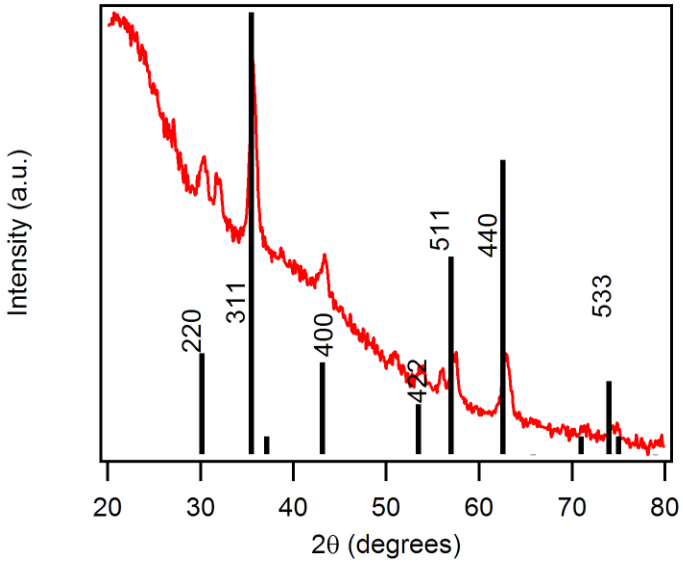

A4.X-ray powder diffraction patterns of CMDx 40COOH coated nanoparticles.

All X-RD powders give sharp XRD peaks, and all prominent peaks (220), (311), (400), (422), (511), (440) and (533) are observed at the corresponding angles in the peak positions. This is well in accordance with the inverse cubic spinel phase Fe_3O_4 (International Centre for Diffraction Data PDF#00-019-0629).

APPENDIX B. ^{1}N-MR Measurements

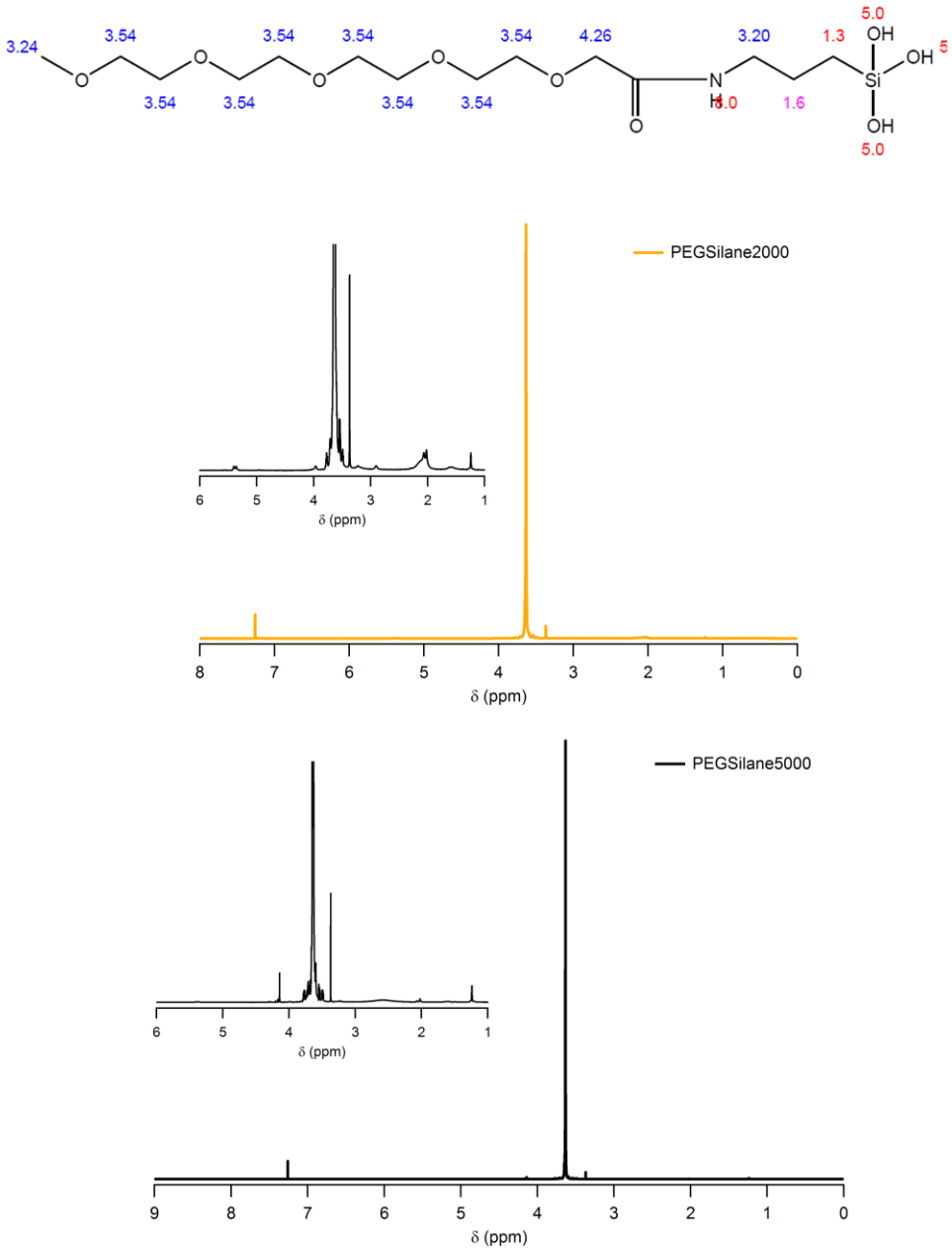

A5.**^{1}H-NMR** analysis for mPEG-silane2000 and mPEG-silane5000 polymers.

APPENDIX C. CMDx with Different Degrees of Substitution of –COOH Groups

A6. CMDx 5 COOH Calculations

mL NaOH	Conc NaOH	mL HCl	Conc HCl	g Dextran	
5	0.0113	3.9	0.01135	0.051	
5	0.0113	3.6	0.01135	0.0516	
5	0.0113	3.3	0.01135	0.0523	
A	0.239901961	0.303100775	0.36414914		
Dsnum	0.038864118	0.049102326	0.058992161		
Dsden	0.980807843	0.975751938	0.970868069		
DS	0.039624599	0.05032255	0.060762283		
COOH	2.445962912	3.10633024	3.750758226	3.10 Average	
				0.65 SD	

A7.CMDx 23 Calculations

mL NaOH	Conc NaOH	mL HCl	Conc HCl	g Dextran	
10	0.0113	1	0.01135	0.052	
10	0.0113	1.1	0.01135	0.0504	
10	0.0113	1.6	0.01135	0.0503	
A	1.954807692	1.994345238	1.885487078		
Dsnum	0.316678846	0.323083929	0.305448907		
Dsden	0.843615385	0.840452381	0.849161034		
DS	0.375382967	0.384416697	0.359706692		
COOH	23.17178809	23.72942576	22.2041168	23.03 Average	
				0.77 SD	

A8.CMDx 40 Calculations

mL NaOH	Conc NaOH	mL HCl	Conc HCl	g Dextran	
10	0.01125	0.3	0.01135	0.0516	
10	0.01125	0.1	0.01135	0.0526	
15	0.01125	0.65	0.01135	0.0519	
A	2.114244186	2.117205323	3.109296724		
Dsnum	0.342507558	0.342987262	0.503706069		
Dsden	0.830860465	0.830623574	0.751256262		
DS	0.412232345	0.412927436	0.670485019		
COOH	25.44644107	25.48934787	41.38796416	30.77 Average	
				9.19 SD	

APPENDIX D. Cell Culture Medium Components – Example: DMEM, PBS

A9.Dulbecco's modified eagle's medium- high glucose (DMEM)

Components	g/L
L-Arginine HCl	0.084
L-Cystine 2HCl	0.0626
L-Glutamine	0.876
Glycine	0.03
L-Histidine HCL H20	0.042
L-Isoleucine	0.105
L-Leucine	0.105
L-Lysine HCl	0.146
Sodium Chloride	6.4
Sodium Phosphate Monobasic	0.109
L-Methionine	0.03
L-Phenylalanine	0.066
L-Serine	0.042
LThreonine	0.095
L-Tryptophane	0.016
L-Tyrosine 2Na 2H2O	0.10379
L-Valine	0.094
Choline Chloride	0.004
Folic Acid	0.004
Glucose	4.5
Sodium Bicarbonate	2.7
Myo-Inositol	0.0072
Niacinamide	0.004
D-Pantothenic Acid	0.0004
Pyridoxal HCl	0.004
Riboflavin	0.0004
Thiamine HCl	0.004
Calcium Chloride	0.2
Ferric Nitrate 9H2O	0.0001
Magnesium Sulfate	0.09767
Phenol Red Na	0.0159
Potassium Chloride	0.4
Niacinamide	0.004
D-Pantothenic Acid	0.0004
Pyridoxal HCl	0.004
Riboflavin	0.0004
Thiamine HCl	0.004
Calcium Chloride	0.2
Ferric Nitrate 9H2O	0.0001
Magnesium Sulfate	0.09767
Phenol Red Na	0.0159
Potassium Chloride	0.4
Niacinamide	0.004
D-Pantothenic Acid	0.0004

A10. Phosphate buffered saline (PBS)

Salt	Concentration (mM)	Concentration (g/L)
NaCl	137	8.01
KCl	2.7	0.20
$Na_2HPO_4 \cdot 2H_2O$	10	1.78
KH_2PO_4	2.0	0.27
pH	7.4	7.4

APPENDIX E. Preliminary Protocol Used to Study Protein-Nanoparticle Interactions Using Commercial CMDx- Coated Nanoparticles with Lysozyme (LYZ) and Bovine Serum Albumin (BSA) Proteins.

Studies for protein-nanoparticle interactions were carried out according to the follow protocol:

a. Prepare stock lysozyme (LYZ) solution adding 12mg of LYZ in 6 mL PBS solution (2mg LYZ/mL concentration).
b. Prepare stock Bovine Serum Albumin (BSA) solution adding 12mg of BSA in 6mL PBS solution (2mg BSA/mL concentration).
c. Prepare stock of commercialCMDx- coated nanoparticles solution of 1.2mgcore/mL concentration adding 0.1816 gr. particles to 15 mL PBS solution (9.91% magnetic core).
d. Place 1mL of stock LYZ solution, and 1mL particle solution in a centrifuge tube (15mL capacity). Triplicate samples.
e. Place 1mL of stock BSA solution, and 1mL particle solution in a centrifuge tube (15mL capacity). Triplicate samples.
f. Place 1mL of PBS solution, and 1mL particle solution in a centrifuge tube (15mL capacity) as a control.
g. Adjust pH samples to 7.3 using KNO_3 0.1M and HNO_3 0.1M
h. Incubate at 37°C for 2 hours.
i. Use 30K ultracentifugation devices at 2000 g for 1 hour at 4°C, to concentrate LYZ solutions until there is approximately 200µL of supernatant.
j. Use 100K ultracentifugation devices at 1000 g for 30 min at 4°C, to concentrate BSA solutions until there is approximately 200µL of supernatant.
k. Recover the supernatant. In order to quantify proteins in solution use UV/vis spectrophotometric measurements at 280 nm (Absorbance = $C*\varepsilon_{protein}*L$, where L= 1cm).
l. Use $\varepsilon_{LYZ\ at\ 280\ nm}$= 37,550 $M^{-1}cm^{-1}$, Mw = 14,388 Da
m. Use $\varepsilon_{BSA\ at\ 280\ nm}$= 43,824 $M^{-1}cm^{-1}$, Mw = 66,400 Da

n. In order to estimate protein adsorption, use the equation:

$$q = \frac{(C_i - C_f)V}{m}$$

Where

q: Protein adsorption mg protein/mg core

V= total volume

C_i= Initial concentration of protein in solution

C_f= Concentration of protein in the supernatant

Reference: Colloids and Surfaces A. Physics Chem. Eng. Aspects. 389 (2011) 97-103.

o. Suspend the particles in 1 mL of Deionized Distilled Water (DDW) with 1.64 KNO3 mM of ionic strength. Sonicate for 10 min to facilitate the suspension.

p. Prepare DLS/Zeta potential solution by adding 333μL of particle solution into 1,667 μL of a solution of 0.27 KNO3 mM of ionic strength).

q. Use DLS and Zeta potential measurements in order to estimate hydrodynamic diameter and surface charge of the protein-nanoparticles samples.

r. Concentrate remnant particles solution in a 150μL TGA crucible the using the TGA oven at 135°C, in order to remove excess water.

s. Perform TGA measurements in an air atmosphere up to 800°C (heating rate 10°C/min). At least 4mg of solid remnant should remain for a successful measurement.

APPENDIX F. Example of Calculations of Protein-Nanoparticle Interactions LYZ-IO 5 (n=4)

1. Calibration curve

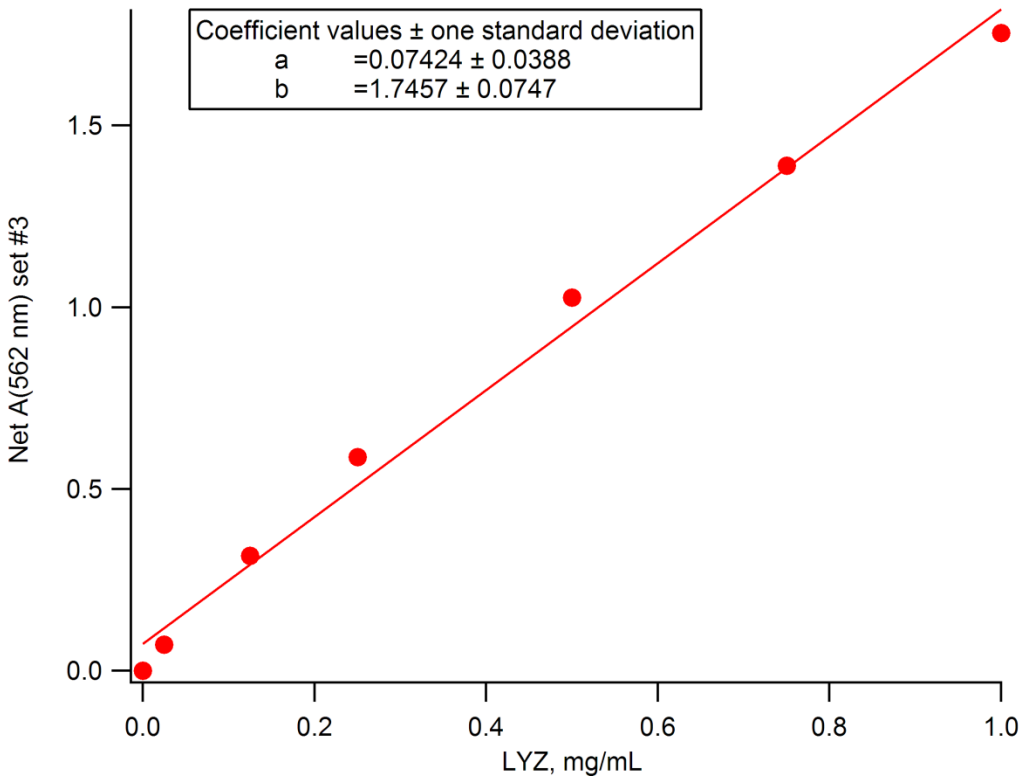

A11. Calibration curve to determine LYZ concentration.

A12. Readings at (562nm) after BCA assay reaction

	A (562nm)	Std deviation	A Net (562nm)	Concentration LYZ, mg/mL
IO 5 LYZ C n=1	1.3897	0.0235	1.3087	0.7071
IO 5 LYZ 1 n=1	0.3073	0.0110	0.2263	0.0871
IO 5 LYZ 2 n=1	0.1027	0.0029	0.0217	0.0000
IO 5 LYZ 3 n=1	0.0837	0.0006	0.0027	0.0000
IO 5 LYZ C n=2	1.4493	0.0451	1.3683	0.7413
IO 5 LYZ 1 n=2	0.3240	0.0098	0.2430	0.0967
IO 5 LYZ 2 n=2	0.1190	0.0010	0.0380	0.0000
IO 5 LYZ 3 n=2	0.0873	0.0021	0.0063	0.0000
IO 5 LYZ C n=3	1.4163	0.0381	1.3353	0.7224
IO 5 LYZ 1 n=3	0.3127	0.0110	0.2317	0.0902
IO 5 LYZ 2 n=3	0.1143	0.0032	0.0333	0.0000
IO 5 LYZ 3 n=3	0.0850	0.0010	0.0040	0.0000
IO 5 LYZ C n=4	1.4783	0.0431	1.3973	0.7579
IO 5 LYZ 1 n=4	0.2720	0.0062	0.1910	0.0669
IO 5 LYZ 2 n=4	0.1195	0.0351	0.0385	0.0000
IO 5 LYZ 3 n=4	0.0870	0.0000	0.0060	0.0000

2. To estimate concentration:

   C_{LYZ} [mg/mL] = Dilution factor*(A Net(562nm) – 0.07424)/1.7457

3. Legend:

   IO 5 LYZ C n=1→ Filtrate obtained from IO 5-LYZ interaction after 1st centrifugation process (1500g, 20 min at room temperature). Sample n=1

   IO 5 LYZ 1 n=1→ Filtrate obtained from IO 5-LYZ interaction after 1st PBS wash (1500g, 20 min at room temperature). Sample n=1

IO 23 LYZ 2 n=1→ Filtrate obtained from IO 5-LYZ interaction after 2nd PBS washed (1500g, 20 min at room temperature). Sample n=1

IO 23 LYZ 3 n=1→ Filtrate obtained from IO 5-LYZ interaction after 3rd PBS washed (1500g, 20 min at room temperature). Sample n=1

4. Initial mass per sample:

C_{LYZ} [mg/mL] = 2*(A Net(562nm) – 0.056156)/1.7073

C_{LYZ} [mg/mL] = 2*(0.8280– 0.056156)/1.7073

C_{LYZ} [mg/mL] = 0.9042

Initial mass LYZ, mg = 0.9042mg/mL * 0.5mL

Initial mass LYZ, mg = 0.4521mg

5. Retention calculations:

Concentration LYZ, mg/mL	n = 1	n = 2	n = 3	n = 4
IO 5 LYZ C	0.6863	0.7205	0.7016	0.7371
IO 5 LYZ 1	0.0871	0.0967	0.0902	0.0669
IO 5 LYZ 2	0.0000	0.0000	0.0000	0.0000
IO 5 LYZ 3	0.0000	0.0000	0.0000	0.0000
Total mass in the filtrated, mg	0.3713	0.3922	0.3801	0.3859
Initial mass, mg	0.4521	0.4521	0.4521	0.4521
Protein interaction, %	17.88%	13.24%	15.93%	14.64%
Average	15.42%			
Std deviation	1.97%			

Steps	n =1	n = 2	n = 3	n = 4	Ave. LYZ retention	StdDev.
Retention after 1st centrifugation	27.13%	23.50%	25.51%	21.74%	24.47%	2.35%
Retention wash 1	17.88%	13.24%	15.93%	14.64%	15.42%	1.97%
Retention wash 2	17.88%	13.24%	15.93%	14.64%	15.42%	1.97%
Retention wash 3	17.88%	13.24%	15.93%	14.64%	15.42%	1.97%

6. Background

	Background C mg/mL
IO 5 C	0.0208
IO 5 1	0
IO 5 2	0
IO 5 3	0
IO 5 SDS	0

Total mass filtrated IO 5 LYZ C n=1:

[C IO 5 LYZ C - C IO 5 LYZ C Background + C IO LYZ 1]* filtrate volume

(0.6863 + 0.0871)mg/mL* 0.48mL = 0.3713mg

Protein interaction, % = (Initial mass – Total mass filtrated)/ Initial mass

Protein interaction, % = (0.4521 – 0.3713)mg/ 0.4521mg

Protein interaction, % = 17.28%

Where: 0.48mL is the filtered volume obtained by Amicon 100K device

Note:

Percent of retention remains constant after 2nd wash step in all LYZ samples, in contrast with BSA samples. After the 3rd wash process BSA can be measured by BCA in the supernatant.

APPENDIX G. Iron determination (by Dr. Lenibel Santiago-Rodriguez)

The assay is based on the complex capabilities of Fe^{2+} to 1,10-phenanthroline, which is colorless before it forms a complex with iron and turns red-orange (508 nm) when it forms a complex with iron.

General Reaction

3 *ortho*-phenanthroline + $Fe^{2+} \rightarrow$ Ferrous tris-*o*-phenanthroline

General Reaction (with chemical structures):

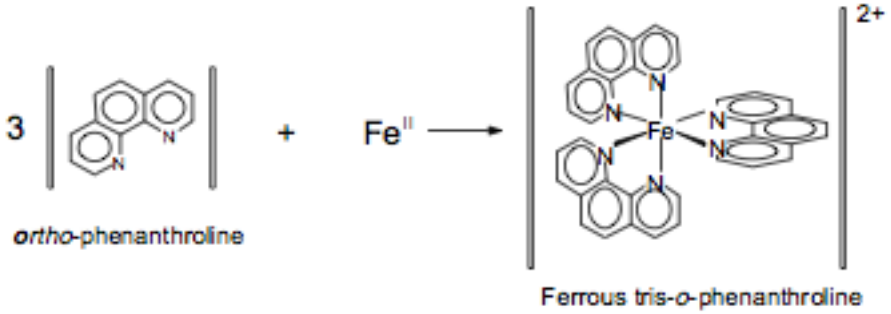

Materials:

1- Iron Standard for ICP 9948 mg/l ± 20 mg/l, Corrosive (Fluka 56209, Lot&pcode BCBB6849 100966354).
2- 1,10-phenanthroline monohydrate ≥99.0%, Very Toxic and Polluting (Fluka 77500, Lot&pcode BCBF1129V 101053288).
3- Hydroxylamine hydrochloride 99.000% trace metal basis, Highly chronic hazard if swallowed, Corrosive, Very Toxic and Polluting (Sigma Aldrich 379921, Lot&pcode MKBH2409V 1001105717).
4- Sodium acetate ≥99.0% (Sigma Aldrich S8750 Lot&pcode 050M0213V 1000917426)
5- DI water, 18.2 MΩ-cm.
6- Microcentrifuge tubes 1.5-1.7 mL Polypropylene with locking lid (Fisher Scientific 02-681-284).

7- Pipettes from Eppendorf Research (2-20 uL (367380Z); 20-200 uL (380867Z); 100-1000 uL (373249Z) and 1-10 mL (348326Z)).
8- E-C Borosilicate Glass Vials 1.5 mL (Fisher Scientific 03-343-3A).
9- Quartz ultramicro cells (Fisher Scientific14-285-928F).

Cleaning of glass vials:

1- Wash each glass vial using a solution of 1x of Triton (Fisher Scientific AC32737) DO NOT use any brush with metal parts.
2- Rinsed each vial at least three times with tap water followed by three more times with distilled water.
3- Completely immerse each vial in 10 % HNO_3 overnight.
4- Rinse each vial the next day with deionized (DI) water (18.2 MΩ-cm).
5- Let the vial dry in a safe place were iron contamination cannot occur.

Validated Methodology for Iron Determination:

Reagents

A- 2.8 g of hydroxylamine in 5 mL of DI H_2O, solubility 56 g/100mL, (8.06 M).
B- 2.0 g of sodium acetate in 20 mL of DI H_2O, solubility 100 mg/mL, (1.22 M).
C- 0.06 g of 1,10-phenanthroline in 23 mL of DI H_2O, solubility 2.6 g/L, (13 mM).
D- Fe Standard solution (9,948 ug/mL).

Preparation of Calibration Curve:

1- A stock solution of iron standard solution was prepared in a concentration of 500 ug/mL from a 9,948 ug/mL solution D (251 ul of reagent D in 4,749 ul of DI water).
2- The stock solutions were used to prepare solutions for the calibration curve (see table below).
3- Finally 10 ul of each stock solution for the calibration curve was added in triplicate to microcentrifuge tubes followed by the addition of 36 ul of DI H_2O and 30 ul of reagent A (0.6 M). Solution was let to reduce for an hour and kept protected from light.
4- 49 ul of reagent B (0.3 M) and 75 ul of reagent C (4.8 mM) were added to each tube.

5- Absorbance at 508 nm was measured.
6- The average of absorbances vs the concentration of iron was plotted and a linear regression was performed (y = mX, this means that your intercept in the y axis should be zero).

Note: Each solution of the calibration curve should be done in triplicates.

A13. Preparation of the stock solution to prepared the calibration curve

Desired Final Iron Content, ug	Desired Final Iron Concentration for the calibration curve, ug/mL	Stock solution of iron used to prepared the stock solutions of the calibration curve, ug/mL	Aliquot of stock solution to prepared the stock solutions of the calibration curve, ul	Aliquot of DI water, ul
0.05	0.250	500	50	4,950
0.1	0.499	500	100	4,900
0.3	1.498	500	300	4,700
0.6	2.996	500	600	4,400
0.9	4.495	500	900	4,100
1	4.994	500	1000	4,000

Preparation of Samples

1- Add the pellet of the cells previously treated with the iron oxide particles in the glass vials.
2- Then add 500 ul of 70% HNO3 (metal trace grade) in a fume hood.
3- Placed the vials in a dry block heater at 101°C overnight (all the solution should be evaporated.
4- Add 46 ul of DI H2O followed by 30 ul of reagent A (0.6 M) to each vial and let the solution to be reduced for an hour protected from light.
5- Then add 49 ul of reagent B (0.3 M) followed by 75 ul of reagent C (4.8 mM) to each vial.
6- Finally the absorbance at 508 nm was measured.

To determine the iron content of iron on the samples the absorbance of each sample need to be corrected using the calibration curve linear regression as follows:

Abs = m * (iron content, ug/mL)

Iron Content, ug/mL = Abs/m